ADVANCING EARTH AND SPACE SCIENCES

JAMES | Journal of Advances in Modeling Earth Systems®

RESEARCH ARTICLE
10.1029/2026MS005795

Key Points:

- Iterative ensemble smoothers improve CLM5 soil moisture calibration by handling nonlinear relations between parameters and observations
- Calibrated parameters showed persistent improvements beyond the assimilation period, confirming model generalization capacity
- Soil moisture estimates improved significantly; evapotranspiration gains were limited, likely due to sparse and noisy observations

Supporting Information:

Supporting Information may be found in the online version of this article.

Correspondence to:

H.-J. Hendricks Franssen,
h.hendricks-franssen@fz-juelich.de

Citation:

Kaandorp, M. L. A., Zhao, H., Poppe Terán, C., Hartick, C., Rigor, P., & Hendricks Franssen, H.-J. (2026). History matching of soil moisture and evapotranspiration over Europe using iterative ensemble smoothers. *Journal of Advances in Modeling Earth Systems*, *18*, e2026MS005795. https://doi.org/10.1029/2026MS005795

Received 2 FEB 2026
Accepted 13 MAY 2026

Author Contributions:

Conceptualization: Mikael L. A. Kaandorp, Harrie-Jan Hendricks Franssen
Data curation: Mikael L. A. Kaandorp, Christian Poppe Terán
Formal analysis: Mikael L. A. Kaandorp, Haojin Zhao
Funding acquisition: Harrie-Jan Hendricks Franssen
Investigation: Mikael L. A. Kaandorp, Haojin Zhao, Christian Poppe Terán

History Matching of Soil Moisture and Evapotranspiration Over Europe Using Iterative Ensemble Smoothers

Mikael L. A. Kaandorp[1,2], Haojin Zhao[1], Christian Poppe Terán[1], Carl Hartick[1,3], Paul Rigor[4], and Harrie-Jan Hendricks Franssen[1]

[1]Forschungszentrum Julich GmbH, Institut für Bio- und Geowissenschaften Agrosphäre (IBG3), Jülich, Germany, [2]Now at European Centre for Medium-Range Weather Forecasts, Bonn, Germany, [3]Deutscher Wetterdienst, Offenbach, Germany, [4]Forschungszentrum Julich GmbH, Jülich Supercomputing Centre (JSC), Jülich, Germany

Abstract Land surface models are crucial components within earth system models, simulating the exchanges of water, energy, carbon, and nitrogen between the land surface, atmosphere, and subsurface. One challenge is the large number of uncertain parameters in these models. One way to calibrate these parameters is by performing history matching, where the model parameters are updated using data assimilation strategies in order to match past observational data more closely. We demonstrate the usage of iterative ensemble smoothers in order to calibrate parameters governing soil moisture and evapotranspiration in the Community Land Model version 5 (CLM5), by assimilating Soil Moisture Active Passive (SMAP) retrievals, and evapotranspiration estimates based on the ICOS flux tower network. With the use of the iterative ensemble smoother we are better able to account for non-linear relations between the model parameters and the observed state vectors compared to only using a single update. We show that model improvements are persistent, with similar improvements in soil moisture for the year 2019 where data were assimilated, as for the year 2020 which was purely used to validate the updated model performance. Substantial model improvements are observed for soil moisture, with neutral to slight improvements for evapotranspiration, which can be attributed to the sparse and noisy nature of these data. By updating model parameters we achieve persistent model improvements and avoid the introduction of model imbalances in state vector updates. This approach can help future studies of terrestrial systems modeling, dealing with coupled models and large numbers of uncertain parameters.

Plain Language Summary Predicting how water moves through soil, and how plants release moisture into the air is important for understanding Earth's climate and ecosystems. Land surface models can be used to simulate these processes on a computer. One difficulty with such models is that they contain many uncertain parameters, which ideally need to be calibrated to make the model predictions as realistic as possible. In our study, we test a method for improving one of these models: the Community Land Model version 5 (CLM5). We adjust the parameters of this model, such that its predictions better match historical measurements of soil moisture taken by satellites, and ground-based measurements of evapotranspiration (the movement of water from land and plants into the air) at various measurement stations over Europe. Our approach uses an iterative technique, where the model parameters are updated multiple times, which helps it handle complex relationships between the parameters and the observed quantities (soil moisture and evapotranspiration). The improved model not only matches the soil moisture observations better for the year on which it is trained (2019), but also produces better predictions for the subsequent year that was used to test the model (2020).

1. Introduction

Understanding and accurately representing the terrestrial water cycle is essential for improving climate predictions and ecosystem and agricultural management. Recent years have seen an increase in the frequency of droughts and heatwaves over Europe (Blunden & Arndt, 2020; Blunden & Boyer, 2021; Markonis et al., 2021; Rousi et al., 2022), which had an effect on the functioning of ecosystems (Graf et al., 2020; Poppe Terán et al., 2023), and which had direct socio-economic impacts (Naumann et al., 2021; Rezaei et al., 2023). As an example, a lack of available water for irrigation, cooling capacity, and fluvial transport resulted in a decrease in productivity in the agricultural, industrial, and transport sectors, causing billions of euros in losses (Naumann et al., 2021; Rakovec et al., 2022). Furthermore, the availability of drinking water was impacted, and extreme heat and low soil moisture enhanced the conditions for catastrophic wildfires (Blunden & Boyer, 2021; Vogel et al., 2019). Due to these devastating impacts it is essential to understand the changing terrestrial water cycle, and how it can be accurately modeled for future projections and assessment of extreme event impacts.

Methodology: Mikael L. A. Kaandorp, Christian Poppe Terán, Harrie-Jan Hendricks Franssen
Project administration: Harrie-Jan Hendricks Franssen
Resources: Harrie-Jan Hendricks Franssen
Software: Mikael L. A. Kaandorp, Carl Hartick, Paul Rigor
Supervision: Harrie-Jan Hendricks Franssen
Validation: Mikael L. A. Kaandorp, Haojin Zhao
Visualization: Mikael L. A. Kaandorp, Haojin Zhao
Writing – original draft: Mikael L. A. Kaandorp, Christian Poppe Terán, Carl Hartick, Paul Rigor, Harrie-Jan Hendricks Franssen
Writing – review & editing: Mikael L. A. Kaandorp, Haojin Zhao, Harrie-Jan Hendricks Franssen

Land surface models play a key role in simulating fluxes of water, energy, and carbon between the land surface and atmosphere (Fisher & Koven, 2020), oftentimes integrated as part of coupled climate or earth system models (Danabasoglu et al., 2020; Guimberteau et al., 2018; Lawrence et al., 2019; Sepulchre et al., 2020). Land surface models are additionally used to capture water and energy fluxes between the land surface and subsurface in hydrological studies (Belleflamme et al., 2023; Naz et al., 2023).

Surface soil moisture is essential to consider in the terrestrial water cycle, as it determines the amount of direct evaporation of soil water into the atmosphere and how much precipitation can infiltrate the deeper layers of the soil (Koster et al., 2019). To accurately capture the terrestrial water cycle, it is furthermore important to correctly represent evaporation. Evaporation accounts for approximately two-thirds of the global terrestrial precipitation but is difficult to measure using remote sensing and, therefore, one of the most uncertain components of the Earth's energy and water balance (Blunden & Arndt, 2020). A substantial fraction of the global terrestrial evaporation is accounted for by transpiration by plants. The exact amount is highly uncertain and depends on the data source and methodology (Rothfuss et al., 2021), with some high-end estimates attributing up to 90% of the global terrestrial evaporation to transpiration by plants (Jasechko et al., 2013), and attributing a smaller remainder to evaporation of water intercepted by plants, soil evaporation, and snow sublimation (Dolman et al., 2014).

Although their ability to simulate ecosystem processes over a heterogeneous landscape and under highly variable conditions is encouraging, land surface models are subject to various challenges and limitations. Model output from land surface models is subject to model uncertainty (due to e.g., simplifications of the underlying physics), uncertainty in inputs (e.g., meteorological forcing, land cover maps), and uncertainty in model parameters (Gao et al., 2021). Recent studies indicate that these uncertainties may lead to discrepancies in the spatiotemporal variability of land surface model outputs compared to observations, particularly for variables such as evapotranspiration, gross primary production, and annual crop yields (Boas et al., 2024; Poppe Terán et al., 2025).

This work uses the Community Land Model, version 5 (CLM5), which contains hundreds of model parameters. Model parameters are often based on empirical evidence from small-scale experiments. For example, the pedotransfer functions in CLM5 that map soil texture to hydraulic parameters are based on the empirical relations in Cosby et al. (1984), where soil samples were used to determine hydraulic properties in the laboratory. The effective parameters at the large (e.g., kilometer) scale might vary substantially due to, for example, subgrid variability and scale dependence (Nykanen & Foufoula-Georgiou, 2001), which poses one of the main difficulties when estimating soil moisture dynamics on a continental scale using coarser model resolutions (e.g., at the kilometer-scale, Samaniego et al. (2013)). One way of dealing with uncertainties in land surface models is by applying data assimilation techniques to get improved estimates of uncertain state variables, uncertain parameters, or both.

Numerous remote sensing products are available that can help to more accurately constrain soil water content in land surface models. Previous data assimilation studies targeting soil moisture have, for example, used Soil Moisture and Ocean Salinity (SMOS) data (Lannoy & Reichle, 2016; Lievens et al., 2015; Muñoz-Sabater et al., 2019; Rodríguez-Fernández et al., 2019), Soil Moisture Active Passive (SMAP) data (Pinnington et al., 2021; Seo et al., 2021; Zhao et al., 2023), and Advanced Scatterometer (ASCAT) data (Dharssi et al., 2011; Muñoz-Sabater et al., 2019; Seo et al., 2021). We choose to use SMAP soil moisture retrievals in this work, given its relatively high correlation and low bias with in situ observations of soil moisture over Europe (Montzka et al., 2017) and its extensive coverage.

In this work, we will furthermore assimilate latent heat flux estimates from eddy-covariance towers, obtained from the Integrated Carbon Observation System (ICOS) Research Infrastructure (Franz et al., 2018; Heiskanen et al., 2022; Pastorello et al., 2020; Warm Winter 2020 Team and ICOS Ecosystem Thematic Centre, 2022), in order to constrain the simulated evapotranspiration. While the extent of these observations is small compared to the SMAP soil moisture observations, they provide continuous, standardized, and quality-controlled records at a high temporal resolution for many locations throughout Europe, and thereby provide valuable information on evapotranspiration for different land cover types. Several prior studies have demonstrated the value of in situ flux or evapotranspiration data for constraining land surface model parameters. For example, Bastrikov et al. (2018) used eddy-covariance measurements of latent heat flux from FLUXNET to optimise parameters controlling latent heat flux (LE) and net ecosystem CO_2 exchange (NEE) in the ORCHIDEE land surface model. Assimilation of FLUXNET measurements has also been applied in Peylin et al. (2016) to constrain carbon fluxes in terrestrial biosphere models using ORCHIDEE. More recently, Bacour et al. (2023) assimilated FLUXNET NEE and LE together with remote sensing products and atmospheric CO_2 observations to assess global carbon fluxes using ORCHIDEE. Latent heat flux and NEE observations from FLUXNET have also been used to optimise ecosystem parameters in the JULES land surface model (Raoult et al., 2016), resulting in substantial improvements relative to default parameter values. Together, these studies highlight the potential of assimilating flux-based observations to constrain key land surface model parameters, providing a strong motivation for incorporating ICOS latent heat flux data alongside soil moisture observations in the present work.

We present several new aspects in this work. We will apply iterative Ensemble Kalman Smoothers to update a large set of parameters related to soil hydrology and evapotranspiration in a land surface model (CLM5) on the continental scale. Iterative ensemble smoothers have not seen extensive usage in land surface models: one example of their application is given in Pinnington et al. (2021), where pedotransfer function parameters were estimated using SMAP soil moisture retrievals. In fields such as reservoir engineering, iterative ensemble smoothers have been used extensively and have been shown to perform well for high-dimensional problems with many observations (Evensen et al., 2019). One benefit of using a smoother algorithm over a filter (e.g., Ensemble Kalman Filters) is the fact that a long time period could be assimilated at once, instead of having short sequential assimilation windows. Previous studies using Ensemble Kalman Filters that included the estimation of model parameters for hydrology and/or land surface models, oftentimes show a slow convergence of the parameter estimates, or no clear convergence at all (Han et al., 2014; Montzka et al., 2011; Moradkhani et al., 2005; Patil et al., 2021). The relatively short assimilation window of filters could mean that parameter updates that are supposed to be time-invariant, compensate for, as an example, seasonally dependent model deficiencies.

We assess whether iterative ensemble smoothers, in this case the Ensemble Smoother with Multiple Data Assimilation (ES-MDA), can be used to constrain land surface model parameters in order to decrease the mismatch with observational data for both soil moisture and evapotranspiration. We will include model parameters that are defined locally (e.g., soil texture), and model parameters that have a global effect (e.g., pedotransfer function parameters that map soil texture to soil hydraulic properties, or parameters related to photosynthesis and plant hydraulics).

By assimilating over a relatively long time period (1 year) we aim to achieve robust parameter estimates that structurally improve the model performance. The use of a smoother means that each parameter is informed by a large set of observations, under varying environmental conditions. Satellite soil moisture retrievals have a penetration depth of a few centimeters, and therefore observe a highly dynamic share of the soil moisture reservoir. Directly updating the soil moisture state vector therefore provides relatively little memory when considering longer (e.g., seasonal) time scales (Gao et al., 2021). By focusing on updating model parameters, instead of directly updating the model state vectors for soil moisture and evapotranspiration, we aim to minimize systematic and long-term model deviations. Our approach of updating model parameters instead of the state vectors directly has the added benefit of avoiding inconsistencies in the state updates, which could lead to water budget imbalances (De Lannoy et al., 2022) and numerical instabilities of the model. The iterative nature of the algorithm is furthermore suitable to resolve possible non-linear dependencies between the model parameters and the observed state vectors (Emerick & Reynolds, 2012)—in our case soil moisture and evapotranspiration.

We will assess the added benefit of jointly assimilating both SMAP and ICOS observations and the effect of separately assimilating both types of observations. Under certain soil saturation conditions, there is a strong relation between soil moisture and the amount of evapotranspiration. This is the case under transitional climate regime conditions (Seneviratne et al., 2010), where the soil saturation lies above the wilting point but still under a critical point where evaporation is controlled by net radiative energy. This can, in turn, lead to a strong coupling between soil moisture and precipitation (Koster et al., 2004). However, various studies have indicated that the assimilation of observations related to soil water content does not necessarily translate into improved evapotranspiration estimates as well (Peters-Lidard et al., 2011), suggesting that additionally constraining Leaf Area Index, vegetation parameters, and parameters governing water uptake by roots might be necessary to achieve this (Strebel et al., 2024). We will investigate whether there is evidence that the strong relationship between soil moisture and evapotranspiration improves soil moisture when assimilating evapotranspiration observations, and vice versa, by assessing the difference in data assimilation performance for arid and moist sites over our domain.

2. Methods

2.1. Model and Domain Description

We use a fork of the Community Land Model, version 5 (CLM5, Lawrence et al., 2019), which simulates the water, energy, and matter balances over a given domain. Our fork of the Community Land Model, eCLM (HPSCTerrSys, 2024b), retains the same model features of CLM5, but uses a different tooling infrastructure, with CMake to build the model, and with custom scripts related to preprocessing and the model configuration. This infrastructure allows for future coupled model runs with hydrological and atmospheric model components within the Terrestrial Systems Modeling Platform (TSMP; HPSCTerrSys, 2024a), for further information see for example, (Gasper et al., 2014; Poll et al., 2025; Shrestha et al., 2014).

The domain in CLM5 is divided into grid cells, which are each further divided into individual land units, consisting of vegetated, urban, glacier, and crop land units (Lawrence et al., 2019). Within each given grid cell the relative area coverage of each land unit is considered. Plants share the same soil column in natural vegetation land units, consequently competing for water. Crops in cultivated land units have separated soil columns and can be managed (irrigated and fertilized) or unmanaged. Natural and cultivated vegetation are characterized using plant functional types (PFT), distinguished by leaf phenology (evergreen or deciduous), morphology (needle or broad leaves, grass, shrubs), and the local climate (temperate, boreal, tropical). The PFT determines which equation and parameters are used to calculate vegetation processes in CLM5. This approach has been used extensively in assessments of the available water resources, carbon budgets, extreme event impacts, and climate change projections on multiple spatial and temporal scales (Boas et al., 2023; Cheng et al., 2021; Lawrence et al., 2019; Sitch et al., 2015; Song et al., 2020; Strebel et al., 2024; Umair et al., 2020; Wozniak et al., 2020; Xie et al., 2020).

Our domain covers Europe using the CORDEX standards (Giorgi et al., 2009), with an approximately equidistant grid spacing of 12 km, or about 0.11°, see also Furusho-Percot et al. (2019). The land surface model parameters were generated using the standard tools included in CLM5. Land cover information, including the distribution of PFTs, was updated to our model resolution using GLC2000 data (Bartholome & Belward, 2005). Climatological Leaf Area Index (LAI) data were obtained from the Copernicus Land Monitoring Service (Copernicus Climate Change Service, Climate Data Store, 2018). Soil properties, such as the percentages of clay and sand were interpolated to the vertical levels of CLM5 using SoilGrids (Shangguan et al., 2017) data.

We use ERA5 data (Hersbach et al., 2020) for the atmospheric forcing of the model. Importantly, this data set generally has a high correlation between the modeled precipitation and gauge-based preciptation observations (Lavers et al., 2022). Besides precipitation, ERA5 data is used to specify the incoming shortwave and longwave radiation, the wind speed, and the air temperature and dewpoint temperature.

2.1.1. Included Parameters

Some recent publications, such as Dagon et al. (2020) and Yan et al. (2023b) have looked at the sensitivity of various state variables in CLM5 (e.g., soil moisture in the upper 10 cm, evapotranspiration, streamflow) to a large number of model parameters. We selected the most sensitive parameters to upper-layer soil moisture and evapotranspiration from these works for perturbation in our experiment.

Soil moisture and evapotranspiration in land surface models are highly sensitive to soil texture, as this determines the resulting soil hydraulic properties such as porosity, hydraulic conductivity, and soil matric potential (Li et al., 2013). CLM5 uses pedotransfer functions to map soil texture (sand, clay, and soil carbon content) to porosity, saturated hydraulic conductivity, and the soil matric potential at saturation. It calculates the hydraulic properties for mineral soil and organic soil separately, after which a weighted average of both quantities is taken based on the fraction of organic soil. Where the sensitivity study in Yan et al. (2023b) directly perturbed soil hydraulic properties using scalar multipliers, we chose to perturb the underlying pedotransfer function parameters instead, as this allows us to consistently and efficiently vary the soil hydraulic properties over our domain.

We base our parameter ranges on the overview from Dagon et al. (2020) as much as possible. We use these parameter ranges to define the 95% confidence interval of the prior parameter values. Where not available, we set the prior 95% confidence interval of the parameters to ±20% around their default value, which is consistent to the perturbation strategy in Dagon et al. (2020). All parameters and their ranges are presented in Table 1.

Table 1
Set of Estimated CLM5 Parameters, the Number of Parameters per Set, and the Parameter Uncertainty Definition

Parameter set	Nr. of parameters	PFT- specific	Range definition
$\alpha_{\theta_s,miner.}$, $\alpha_{b,miner.}$, $\alpha_{\psi_s,miner.}$, $\alpha_{k_s,miner.}$	4		Section S1 in Supporting Information S1
$\beta_{\theta_s,miner.}$, $\beta_{b,miner.}$, $\beta_{\psi_s,miner.}$, $\beta_{k_s,miner.}$	4		Section S1 in Supporting Information S1
$\rho_{sc,\max}$	1		±20%
$\theta_{s,om}$, $k_{s,om}$, $\psi_{s,om}$, b_{om}, $\Delta_{z,\theta,om}$, $\Delta_{z,\psi,om}$, $\Delta_{z,b,om}$	7		±20%
Δ_{sand}, Δ_{clay}, Δ_{om}	1242		±20%
$f_{sat,decay}$	1		(Dagon et al., 2020)
α_{g_s}	9	x	(Dagon et al., 2020)
β_{g_s}	9	x	±20%
J_{maxb0}, J_{maxb1}, $t_{c,j0}$, H	4		±20%
$k_{\max}$	9	x	(Dagon et al., 2020)
$H_2O_{can.,max}$	1		(Dagon et al., 2020)

Note. All parameters are defined in the main text, Section 2.1.1.

The pedotransfer functions for mineral soil in CLM5 are based on Clapp and Hornberger (1978) and Cosby et al. (1984), mapping sand and clay percentages to the porosity θ_s, the saturated hydraulic conductivity k_s (mm s^{-1}), the saturated soil matric potential ψ_s (mm), and the Clapp and Hornberger coefficient b.

There are eight empirical regression coefficients based on Cosby et al. (1984) that map the sand and clay percentages to the mineral soil hydraulic properties in CLM5, consisting of four slope parameters α ($\alpha_{\theta_s,miner.}$, $\alpha_{b,miner.}$, $\alpha_{\psi_s,miner.}$, $\alpha_{k_s,miner.}$) and four intercept parameters β ($\beta_{\theta_s,miner.}$, $\beta_{b,miner.}$, $\beta_{\psi_s,miner.}$, $\beta_{k_s,miner.}$):

$$\theta_{s,miner.} = \alpha_{\theta_s,miner.}(\%_{sand}) + \beta_{\theta_s,miner.}, \tag{1}$$

$$b_{miner.} = \alpha_{b,miner.}(\%_{clay}) + \beta_{b,miner.}, \tag{2}$$

$$\psi_{s,miner.} = -10 \times 10^{\alpha_{\psi_s,miner.}(\%_{sand})+\beta_{\psi_s,miner.}}, \tag{3}$$

$$k_{s,miner.} = 0.0070556 \times 10^{\alpha_{k_s,miner.}(\%_{sand})+\beta_{k_s,miner.}}, \tag{4}$$

where the prefactors in (Equations 3 and 4) are used to convert from cm to mm, and from inches per hour to mm s^{-1} respectively. We used the raw data from Cosby et al. (1984) to estimate the coefficients α and β, as well as their uncertainties which are used to define the prior parameter ranges in the data assimilation procedure. See Section S1 in Supporting Information S1 for further explanation.

The calculation of hydraulic properties for organic soil in CLM5 is described in Lawrence and Slater (2008). The soil organic fraction is calculated by dividing the soil carbon density ρ_{sc} by the maximum soil organic density $\rho_{sc,\max}$. The standard value of the parameter $\rho_{sc,\max}$ is set to 130 kg m^{-3} in CLM5. We observed that this parameter has a large influence on soil moisture, especially in the upper latitudes where the soil organic density reaches $\rho_{sc,\max}$ in the upper soil layers (i.e. a soil organic fraction of 1). We therefore include $\rho_{sc,\max}$ as a parameter in our study, using the standard 95% confidence interval (±20%) to perturb it. We furthermore perturb the hydraulic properties of the organic soil itself, which in CLM5 are based on a peatland study by Letts et al. (2000). Hydraulic properties of the organic soil are defined at the surface, and vary until reaching a depth of 0.5 m. We perturb the surface parameters ($\theta_{s,om}$, $k_{s,om}$, $\psi_{s,om}$, b_{om}) and the depth increments ($\Delta_{z,\theta,om}$, $\Delta_{z,\psi,om}$, $\Delta_{z,b,om}$; $k_{s,om}$ is not included as this is set to $k_{s,miner.}$ for deeper soil layers in CLM5).

We introduce depth-invariant spatial perturbation fields to the soil texture components: the percentage sand (Δ_{sand}), percentage clay (Δ_{clay}), and soil carbon content (Δ_{om}). The standard 95% confidence interval (±20%) is used to perturb the three soil components. This perturbation magnitude is plausible given the variation in soil texture between different soil property databases (Stoorvogel & Mulder, 2021). We introduce the soil texture perturbations every 16th grid cell, based on the correlation length scale calculated from the SMAP soil moisture observations. The perturbation field at intermediate grid cells is calculated using radial basis functions with an exponential kernel, see Section S2 in Supporting Information S1 for further clarification. This approach keeps the number of soil texture perturbation parameters limited, while allowing for local corrections to the soil texture when necessary.

Parameterization of runoff has a strong influence on soil moisture (Yan et al., 2023a). The runoff calculation in CLM5 is dependent on the saturated fraction of a grid cell, which is determined by the water table depth and a decay factor $f_{sat,decay}$ (Niu et al., 2005). This decay factor is included in our parameter perturbations, where we use the parameter bounds as given in Dagon et al. (2020).

Various previous studies on land surface models have shown a high sensitivity of evapotranspiration and soil moisture in the upper few centimeters to stomatal conductance and photosynthesis parameters (Dagon et al., 2020; Jefferson et al., 2017; Li et al., 2013). CLM5 uses the stomatal conductance model by Medlyn et al. (2011), where the stomatal conductance is calculated such that carbon gain (photosynthesis) is maximized, while minimizing water loss. The stomatal conductance g_s (μmol m^{-2} s^{-1}) is calculated based on the leaf-to-air vapor pressure deficit D (kPa), the leaf net photosynthesis A (μmol m^2 s^{-1}), the CO_2 partial pressure at the leaf surface c_s (Pa), and the atmospheric pressure P_{atm} using

$$g_s = \beta_{g_s} + 1.6\left(1 + \frac{\alpha_{g_s}}{\sqrt{D}}\right)\frac{A}{c_s/P_{atm}}, \tag{5}$$

where the α_{g_s} and β_{g_s} parameters can be set for every PFT separately in CLM5. We allow both parameters to vary for every modeled PFT in our simulations, where we use the expert-based parameter ranges from Dagon et al. (2020) for α_{g_s}. We use the standard 95% confidence interval (±20%) to vary β_{g_s}. The CLM5 photosynthesis module LUNA includes four parameters (Ali et al., 2016), which we allow to vary all: the baseline proportion of nitrogen allocated for electron transport rate J_{maxb0}, the electron transport rate response to light availability J_{maxb1}, the baseline ratio of Rubisco limited rate to light $t_{c,j0}$, and the electron transport rate response to relative humidity H (all unitless). We set the prior 95% confidence interval of these parameters to ±20% around their baseline values.

Plant hydraulic conductivity has a large influence on transpiration by plants in land surface models. Hydraulic conductivity is calculated for four different plant segments in CLM5: the root, stem, shaded leafs, and for sunlit leafs. Water supply in the plant segments is modeled via Darcy's law, where the hydraulic conductance for each segment is determined though xylem vulnerability curves (Tyree & Sperry, 1989). The parameter $k_{\max}$ determines the maximum conductance, which has been observed to have a large influence on evapotranspiration and upper layer soil moisture (Dagon et al., 2020). We allow $k_{\max}$ to vary per PFT in our simulations, using the parameter bounds as given in Dagon et al. (2020). The value for $k_{\max}$ is set uniformly for all plant segments for a given PFT, as is also done in the standard CLM5 setup.

Evapotranspiration is furthermore highly influenced by the amount of canopy water stored on leaf surfaces (Yan et al., 2023a). We include the maximum canopy water storage $H_2O_{can.,max}$ as a parameter, using the parameter bounds given in (Dagon et al., 2020).

2.2. Training and Testing Data Sets

We use SMAP soil moisture retrievals (Entekhabi et al., 2014) and ICOS flux tower evapotranspiration estimates (Franz et al., 2018) to calibrate the parameters listed in Table 1. Data for the years 2019 and 2020 are used, where we first calibrate the parameters based on one year of data from 2019, and then validate the model performance over the year 2020, to see whether the improvements remain consistent over time. By using a full annual cycle for model calibration and keeping the parameters fixed in time, we aim to obtain parameter estimates that are not biased toward specific seasons, but instead reflect the dominant annual variability driven by key processes such as vegetation phenology and surface energy partitioning. Using 1 year of data that spans a complete seasonal cycle has been shown to be sufficient to constrain land surface model parameters, and is consistent with previous land surface model calibration studies focusing on soil moisture (e.g., Loaiza Usuga & Pauwels, 2008; Pinnington et al., 2021).

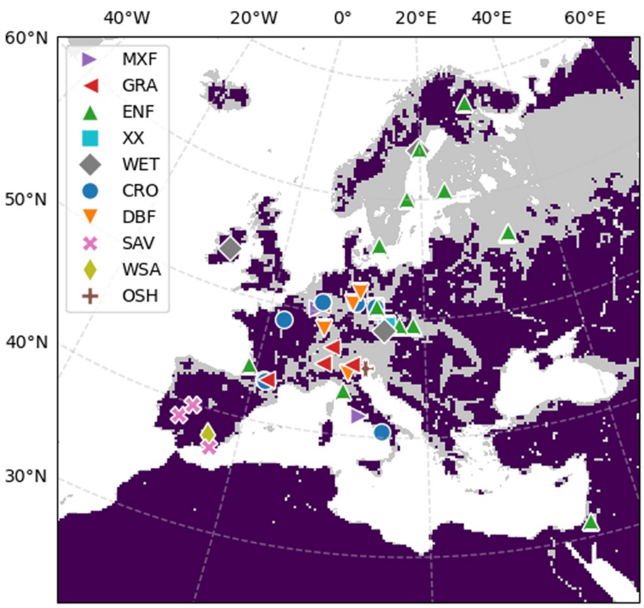

Figure 1. Availability of SMAP observations (dark shading) and ICOS observations (colored symbols). For each of the ICOS observation sites the landcover type is indicated by the different symbols/colors.

2.2.1. SMAP

For the soil moisture observations we use the SMAP enhanced Level-3 soil moisture product at a 9 km resolution (O'Neill et al., 2020). The spatial data coverage of the SMAP soil moisture retrievals is presented in Figure 1 using the dark blue shading. We only use SMAP retrievals where the quality flags are favorable, which means that retrievals for densely vegetated areas, regions with snow, ice, and/or frozen ground, and mountainous areas are not used. We specify a standard deviation of 0.04 $cm^3\ cm^{-3}$ for the SMAP retrievals, according to the baseline requirement under favorable observational conditions (Entekhabi et al., 2014).

2.2.2. ICOS

The Integrated Carbon Observation System (ICOS) consists of a network of eddy covariance (EC) measurement towers across the European continent (ICOS RI, 2022). In short, these EC towers are equipped with instruments to determine the wind, gas, energy, and momentum data, from which key fluxes can be determined. These include, for example, the sensible and latent energy fluxes between the atmosphere and land surface, and carbon uptake and emissions by ecosystems. While the EC method is regarded as an appropriate standard to measure energy and carbon fluxes on the ecosystem level (Aubinet et al., 2012; Pastorello et al., 2020), several uncertainties still persist. These include, for example, a variable footprint area of the tower, which varies depending on wind direction, wind speed, and land surface heterogeneity (Chu et al., 2021). A missing representation of large eddies in the measurements can furthermore result in inconsistencies in the energy balance (Eshonkulov et al., 2019; Franssen et al., 2010; Zhang et al., 2024).

For this work, we extracted energy balance corrected latent heat (LE_CORR), which is post-processed from the directly measured latent heat from the ICOS Warm Winter 2020 data set (ICOS RI, 2022), including 70 sites over the European continent. The energy balance closure is accomplished by re-partitioning of the missing energy over latent and sensible heat fluxes according the observed Bowen ratio. Latent heat in W m^{-2} is transformed to ET in mm day^{-1} by multiplying with the factor 0.035, assuming a constant enthalpy of vapourization decoupled from variable temperature, given its negligible influence on the overall outcome of the conversion (Allen, 2000).

The spatial coverage of the ICOS flux tower network we used is presented in Figure 1 using the colored symbols, where each symbol/color represents the landcover type of each flux tower footprint. For most of the ICOS measurement sites the landcover type is specified, which fall into 9 categories over our domain: Croplands (CRO), Mixed Forests (MXF), Grasslands (GRA), Evergreen Needleleaf Forests (ENF), Permanent Wetlands (WET), Deciduous Broadleaf Forests (DBF), Savannas (SAV), Woody Savannas (WSA), Open Shrublands (OSH). In case the land cover type was not specified in the metadata platform we define the landcover type as Unspecified (XX).

In our model setup we consider nine different plant functional types: (a) Needleleaf Evergreen Trees, (b) Needleleaf Deciduous Trees, (c) Broadleaf Evergreen Trees, (d) Broadleaf Deciduous Trees, (e) Broadleaf Evergreen Shrubs, (f) Broadleaf Deciduous Shrubs, (g) Grass, (h) Crops, and (i) Irrigated Crops.

For some of the dominant landcover types as reported for the ICOS flux tower sites, we can directly compare the evapotranspiration estimates with the modeled CLM5 output at the PFT level (GRA, ENF, DBF map to PFT's 7, 1, 4, respectively). For other landcover types that are not directly represented by CLM (e.g., Mixed Forests, Savannas) we mapped the landcover type to the most similar PFT, or the mean of similar PFT's. For the landcover types WET and XX we did not have evapotranspiration estimates available at the PFT level: in those cases we used the modeled evapotranspiration at the gridcell level instead. The ICOS land cover type mapping to CLM5 PFT is presented in Table 2.

Table 2
Map From the Dominant Landcover Type at the ICOS Flux Tower Sites, to the PFT's That Were Used in CLM5 to Determine the Corresponding Modeled Evapotranspiration

ICOS landcover type	PFT used in CLM5
CRO	8
MXF	1,4
GRA	7
ENF	1
WET	cell avg.
DBF	4
SAV	7
WSA	6
OSH	5,6
XX	cell avg.

2.3. Iterative Ensemble Smoother

We use the Ensemble Smoother with Multiple Data Assimilation (ES-MDA, Emerick & Reynolds, 2013) to assimilate the SMAP and ICOS observations into the model, where the model parameters to be calibrated are listed in Table 1. The ES-MDA algorithm is similar to the Ensemble Smoother (ES) algorithm (Evensen & van Leeuwen, 2000), with the only difference being that the observational data are assimilated multiple times. The main motivation for using this algorithm is that by using multiple iterations, we should be better able to account for nonlinear relations between the model parameters and the observed state vectors (Emerick & Reynolds, 2012), which are in this case soil moisture and evapotranspiration.

We base the general ES-MDA implementation on Emerick (2016). The update step of ensemble member j at iteration i can be written as

$$\mathbf{m}_j^a = \mathbf{m}_j^f + \mathbf{C}_{\mathrm{MD}}^f\left(\mathbf{C}_{\mathrm{DD}}^f + \alpha_i \mathbf{C}_{\mathrm{D}}\right)^{-1}\left(\mathbf{d}_{\mathrm{obs},j} - \mathbf{d}_j^f\right), \tag{6}$$

where $\mathbf{m}$ is the vector containing the model parameters, $\mathbf{d}_{\mathrm{obs}}$ is a vector containing the observational data, and $\mathbf{d}$ contains the data predicted by the model. The superscripts f and a refer to the forecast (prior) and analysis (posterior) respectively. The matrix $\mathbf{C}_{\mathrm{MD}}$ contains the cross-covariances between the prior model parameters $\mathbf{m}^f$ and predicted data $\mathbf{d}^f$, and $\mathbf{C}_{\mathrm{DD}}$ contains the auto-covariances of the predicted data $\mathbf{d}^f$. We assume the observational errors are uncorrelated, making the observation error covariance matrix $\mathbf{C}_{\mathrm{D}}$ diagonal. Finally, a choice for the inflation factors α_i needs to be made. Various methods exist in the literature, where we chose the Hanke's regularization condition approach from Rafiee and Reynolds (2017) to calculate a geometric series for α_i, as this was shown to result in relatively little overfitting of parameters. The inflation factors are determined prior to starting the history matching procedure, and depend on the eigenvalues of the problem and the number of ES-MDA iterations. We will investigate how the number of iterations changes the results, by performing a set of experiments with 1, 3, 5, and 7 ES-MDA iterations.

Localization is required for our problem (Chen & Oliver, 2017), given the relatively large number of parameters compared to the ensemble size that we can computationally afford (64 ensemble members). We apply a radius-based localization in space for the parameters with a defined location (Δ_{sand}, Δ_{clay}, Δ_{om}, see Table 1). We use a Gaspari-Cohn localization function, with its radius defined by the soil moisture correlation length scale, see Section S2 in Supporting Information S1.

Estimating a mix of global and localized parameters can lead to complications such as too strong updates of global parameters, as discussed in Malartic et al. (2022). We use the same approach as in Malartic et al. (2022), with a global tapering factor ζ that dampens the global parameter updates. We ran a set of five test experiments where we assimilated a period of 3 months with generally high biological productivity over Europe (May–July 2019), with four different values for ζ ranging from 0.2 to 1.0. In these tests we used a total of 3 ES-MDA iterations. Ideally, one would compare a large set of values for ζ for a varying number of total iterations and a varying number of ensemble members. However, this was computationally infeasible, so we opted for this approach to hopefully get reasonably close to optimal performance. In the end we chose $\zeta = 0.4$ which gave the lowest RMSE with respect to both the SMAP and ICOS observations, see Section S3 in Supporting Information S1. Without this tapering factor (i.e., $\zeta = 1$), global parameter updates tended to be very large, resulting in unrealistic parameter values and unstable simulations.

Running the ES-MDA algorithm requires the storage of soil moisture and evapotranspiration observations and state estimates over the whole assimilation window, in this case 1 year. Based on limitations regarding memory and computational performance, we chose to thin the SMAP observations, only using SMAP retrievals once every 3 days. For ICOS we use all available data. This resulted in the assimilation of approximately 1,000,000 SMAP observations and 4,700 ICOS observations over the year 2019. Based on computational constraints, we choose an ensemble size of 64 members.

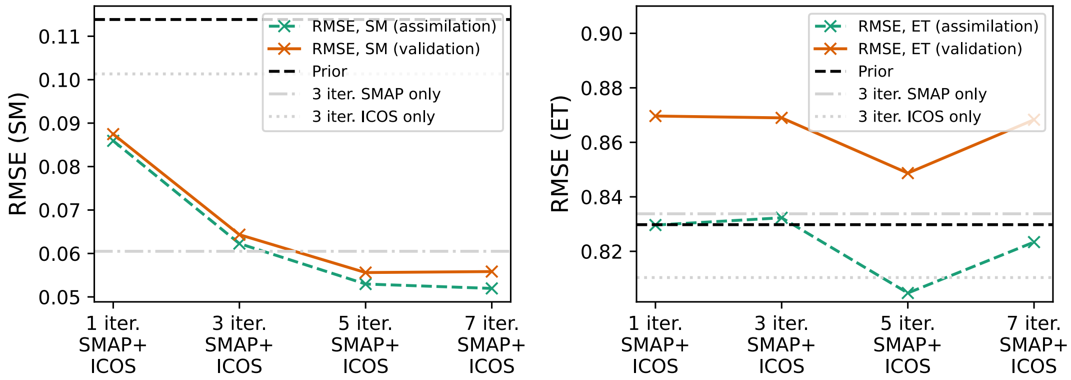

Figure 2. Model performance in terms of root mean squared error, for a varying number of total iterations and varying assimilated data sets. The RMSE of soil moisture (CLM vs. SMAP) is presented in the left panel, the RMSE of evapotranspiration (CLM vs. ICOS) is presented in the right panel. Results for a varying number of total iterations of the ES-MDA algorithm are presented using the colored solid lines. Horizontal lines indicate the model performance when using the prior model parameters, and when assimilating SMAP/ICOS separately.

The ES-MDA algorithm (Equation 6) is equivalent to using a standard ensemble smoother when having a linear forward solver (Emerick & Reynolds, 2012; Köpke et al., 2019). By distributing the assimilation over multiple iterations with inflated observation error covariance, ES-MDA reduces the impact of the linearization implicit in a single ensemble smoother update (Evensen et al., 2022), and is therefore better suited to capture non-linear relationships between the model parameters and the state variables (soil moisture and evapotranspiration). We investigate whether using multiple iterations (3, 5, or 7) improves performance relative to a single iteration, which is equivalent to applying a standard ensemble smoother (Evensen et al., 2024). We do not separately test an Ensemble Kalman Filter (EnKF) configuration, in which observations are assimilated sequentially over smaller sub-windows of the assimilation period. For linear and Gaussian problems, the EnKF and the ensemble smoother are theoretically equivalent in the sense that they converge to the same posterior parameter estimates at the final time (Evensen & van Leeuwen, 2000). As a result, the ensemble smoother is a more natural choice for the history matching problem considered here, providing consistent parameter estimates over the full assimilation window.

3. Results and Discussion

3.1. Selecting the Optimal Model Performance

In a set of assimilation experiments we looked at the effect of varying the number of ES-MDA iterations, and at the effect of assimilating SMAP and ICOS observations together versus separately. We used a 1-year assimilation window for the year of 2019, using 64 ensemble members.

After finishing the assimilation window, we used a validation window of 1 year to test whether posterior parameter values perform well for the subsequent year as well. In Figure 2 we present the model performance in terms of RMSE for different setups of the ES-MDA algorithm, each with a different number of total iterations. The presented results should not be interpreted as consecutive steps of the ES-MDA algorithm, but as separate setups with a different number of specified iterations counts, and corresponding inflation factors α, see Equation 6. In the same figure, we furthermore look at the effect of assimilating SMAP and ICOS observations only, as opposed to assimilating both data sets simultaneously.

We find a substantial decrease in soil moisture RMSE already with one iteration of the ES-MDA algorithm (i.e., equivalent to running a "standard" ensemble smoother algorithm). However, the RMSE decreases further when using 3 and 5 iterations. No substantial improvement in the soil moisture RMSE is observed when increasing the number of iterations from 5 to 7. The results for the training window and validation window lie very close together, indicating that improvements in the soil moisture for the year 2019 structurally improve the results for the year 2020 as well. The pattern for the RMSE of evapotranspiration is slightly different. We see a similar RMSE for the prior parameter values and when using 1 or 3 iterations. Results are improved the most when using 5 iterations, and worsen in the case of using 7 iterations. This can have multiple causes. One possibility is the iterative algorithm getting stuck in a local minimum. Furthermore, as addressed in for example, Emerick (2019)

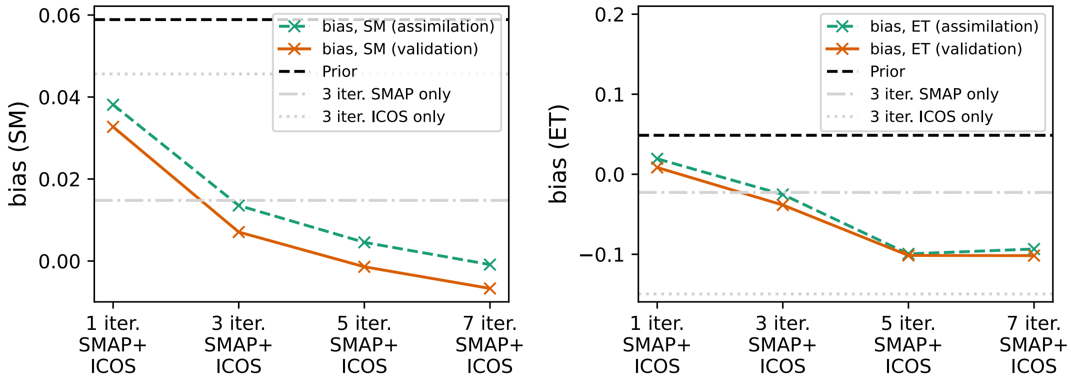

Figure 3. Model bias for a varying number of iterations and varying assimilated data sets. The soil moisture bias (CLM vs. SMAP) is presented in the left panel, the evapotranspiration bias (CLM vs. ICOS) is presented in the right panel. Results for a varying number of total iterations of the ES-MDA algorithm are presented using the colored solid lines. Horizontal lines indicate the model performance when using the prior model parameters, and when assimilating SMAP/ICOS separately.

and Emerick and Neto (2023), the ES-MDA algorithm can have a tendency to overcorrect parameters and to overfit the data, resulting in a too low ensemble spread, which in turn can lead to a decreased performance.

A good improvement in the soil moisture model bias is observed, see Figure 3. A wet bias of -0.054 cm^3 cm^{-3} is present for the prior parameter settings, changing into a negligible dry model bias of 0.001 cm^3 cm^{-3} when using 5 iterations, both for the assimilation window and the validation window. The model bias for evapotranspiration is already relatively low for the prior parameter settings, with a slight model overestimation of 0.05 mm d^{-1}, moving to a slight underestimation of 0.10 mm d^{-1} when using 5 iterations for the validation window.

We present additional analysis for the Pearson R correlation coefficient for the different assimilation setups in Section S4 of the Supporting Information S1. The trends for the Pearson R correlation coefficient are similar to the ones for RMSE, attaining high values for 5 iterations when assimilating both SMAP and ICOS data ($R = 0.84$ for SMAP, $R = 0.79$ for ICOS, for the validation window).

The model performance when assimilating only SMAP data, or when only assimilating ICOS data is presented in Figures 2 and 3 using the gray horizontal lines. We find that when only assimilating SMAP data there is no substantial improvement in the evapotranspiration estimates. When assimilating ICOS data only, we do see a slight improvement in the soil moisture RMSE and bias, although the effect is only minor (the RMSE for the validation window decreases from 0.12 cm^3 cm^{-3} to 0.11 cm^3 cm^{-3}). These small improvements are consistent over the entire domain, with small reductions in the RMSE and bias across all latitudes, both for the assimilation and validation window, see Figure S7 in Supporting Information S1. Only in the southern-most part of the domain (<20°N) there is no reduction in the RMSE and bias: here the prior mismatch with respect to the SMAP retrievals (RMSE: 0.03) is already below the expected accuracy under favorable conditions 0.04 cm^3 cm^{-3}.

Under certain atmospheric conditions there can be a strong relation between soil moisture and evapotranspiration (Seneviratne et al., 2010). Under energy-limited conditions evapotranspiration is not sensitive to changes in soil moisture content: in such a case it is unlikely that the assimilation of ICOS data results in an improvement in modeled soil moisture, and vice-versa for the assimilation of SMAP data. We assessed the difference in DA performance for arid (i.e., generally water-limited) and moist (i.e., generally energy-limited) ICOS sites over our domain during the calibration period (2019) using SMAP SM and ICOS ET observations (see Section S5 in Supporting Information S1). Results are analyzed across different aridity regimes (Zomer et al., 2022), and classified by season. For ET, the impact of DA exhibits a strong dependence on aridity and season. ET RMSE reductions are generally larger in arid regions, with the strongest improvements occurring during summer for both SMAP-only and FLX-only assimilation experiments. In humid regions, ET improvements are smaller and more variable, indicating a reduced sensitivity of ET to SM corrections.

SM generally shows clear improvement relative to the open-loop simulations across DA scenarios, with RMSE reductions that are again most pronounced in arid regions, particularly during summer. However, SM improvements from the FLX-only assimilation are weak overall and absent in humid regions, whereas

SMAP + FLX and SMAP only DA yield clearer benefits. These results indicate that arid, water-limited regions benefit more from DA for both for SM and ET. This behavior likely reflects stronger SM-ET coupling in arid environments, where soil water availability exerts a dominant control on ET. In humid regions, ET is also strongly controlled by atmospheric vapor pressure deficit and vegetation (Baldocchi et al., 2022; Zhang et al., 2023), limiting the effectiveness of DA from SM alone.

Model limitations may partly explain why assimilating ICOS data alone leads to only modest improvements. For example, evapotranspiration estimates depend on plant functional type (PFT), for which only a limited number of categories are represented in our model. In addition, the spatial coverage of ICOS sites is sparse and uneven across the domain, with most stations located in the central region. This limited and clustered coverage reduces the ability of the calibration to improve RMSE at the domain scale, particularly when compared to SMAP soil moisture observations, which provide much broader spatial coverage.

In the next sections we will focus on the results when using 5 iterations of the ES-MDA algorithm, which showed the most improvement in RMSE for the mismatch of both SMAP and ICOS data. We will evaluate the mismatch in soil moisture and evapotranspiration separately in the next sections.

3.2. Soil Moisture

The average deviation between the modeled volumetric soil moisture and the SMAP soil moisture retrievals after 5 iterations of the ES-MDA algorithm is plotted in Figure 4. We observe a wet model bias over most of Europe for the prior model run, a dry bias over the Nordic countries, and a strong wet bias in the north-eastern part of the domain between 60°N—70°N and 40°E—60°E. These biases are greatly reduced for the posterior model run (right column of Figure 4), with large areas having a deviation less than 0.05 $cm^3\,cm^{-3}$. Improvements are furthermore consistent for both the assimilation window and the validation window, indicating that structural improvements are made with respect to the overall modeled soil moisture. A large part of the improvements can be attributed to changes in the soil texture (Δ_{sand}, Δ_{clay}, Δ_{om} in Table 1) after the assimilation, which will be further discussed in Section 3.5.

While over most parts of the domain the model bias with respect to SMAP is reduced, we do see an increase in the mismatch over the island of Ireland. Furthermore there is a persistent dry model bias visible over Tunisia, which could be caused by difficulties to model this particular area, as it contains a large salt-covered depression that is only flooded during some months (Abdallah et al., 2016).

The improvement of the posterior model performance is clearly visible in the density plots of the SMAP soil moisture retrievals versus the modeled soil moisture in Figure 5. We see a consistent reduction in RMSE and model bias for all latitude bands of the domain, both for the assimilation and validation window. Over the entire domain, there is a decrease in the Root Mean Square Error (RMSE) from 0.12 $cm^3\,cm^{-3}$ to 0.06 $cm^3\,cm^{-3}$, and a decrease in the bias from 0.05 $cm^3\,cm^{-3}$ to 0.00 $cm^3\,cm^{-3}$ over the validation window, and an increase in the Pearson correlation coefficient from 0.68 to 0.84. The reduction in RMSE is the greatest for 60°N–70°N, where the wet model bias in the north-eastern part of the domain leads to a high RMSE for the prior model parameters. This cluster of points with a wet model bias moves closer to the 1:1 line for the posterior model parameters. Overall, the soil moisture of the posterior model runs is centered more densely around the 1:1 line, as indicated by the increased data count densities in the different panels.

Figure 6 presents a timeseries of the mean deviation between the CLM model output and the SMAP soil moisture retrievals. The time series are presented per latitude band, where for each date the spatial mean of the deviation was calculated. Generally, the deviation is closer to zero after the data assimilation. The target accuracy of SMAP (0.04 $cm^3\,cm^{-3}$, Entekhabi et al. (2014)) is plotted as a reference using the red dashed lines.

Little deviation is present for the lowest latitude band between 20°N and 30°N in both the OL and DA simulations. Most deviation can be observed for the highest latitude band, between 60°N and 70°N. Most of the deviation occurs either when the ground starts to be frozen (around October-November), or at the onset of thaw (around April-May). Since less measurements are available for this latitude band around these periods (large areas are still covered by snow), single deviating points have a large influence on the overall mean deviation. The mean deviation between 60°N and 70°N is relatively small for the remainder of the available months (between May and October). However, the model generally remains dryer than the SMAP soil moisture retrievals for the Nordic

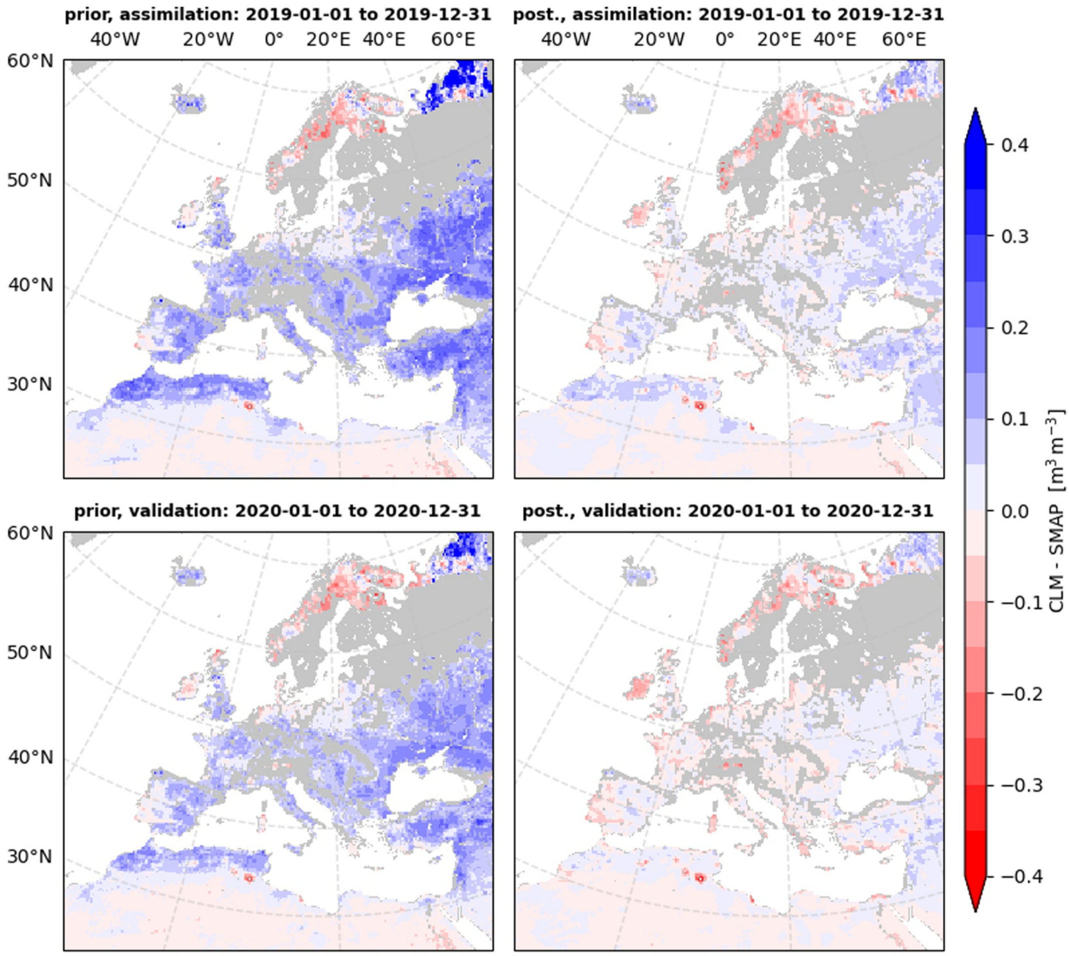

Figure 4. Average mismatch between the SMAP soil moisture retrievals and modeled CLM values. In red areas the model output is dryer than the SMAP retrievals, in blue areas the model output is wetter than the SMAP retrievals. Left column: open loop simulations, right column: after the data assimilation procedure. Upper row: training window, lower row: validation window.

countries, and wetter for the Russian tundra (see also Figure 4), with both deviations roughly canceling each other out in the time series in Figure 6.

Deviations between the model (CLM) and the SMAP soil moisture retrievals can either occur because of inaccuracies in the retrievals themselves, or due to model deficiencies. SMAP has been observed to underestimate soil moisture under frozen conditions, where the dielectric constant of the soil can reduce to levels similar to dry soil, and has been observed to overestimate soil moisture at the end of dry spells compared to in situ observations (van der Velde et al., 2021). This can lead to a lower accuracy than the target accuracy (e.g., 0.06 $cm^3\ cm^{-3}$ in the Netherlands (van der Velde et al., 2021) vs. the target accuracy of 0.04 $cm^3\ cm^{-3}$). The accuracy of SMAP in the northern latitudes is furthermore likely reduced due to limitations in the soil dielectric model for organic soils (Park et al., 2019); as well as transient waterbodies in the northern permafrost regions that could impact the accuracy of the SMAP soil moisture retrievals (Yi et al., 2022).

On the other hand, the model also carries significant uncertainties. When considering the northern part of the domain, model uncertainties related to the snow cover extent and snow water equivalent (Largeron et al., 2020) translate to uncertainties in soil moisture at the onset of thaw. Additionally, uncertainties in soil organic content and its hydraulic properties will have a large influence on soil moisture for the high latitudes, given the high soil carbon content in this region (see Figure 15a). The inclusion of organic soil is characterized by lower soil temperatures in summer and slightly higher soil temperatures in winter, due to a relatively low thermal conductivity and a high heat capacity. Furthermore, organic soils have a high porosity and hydraulic conductivity,

10.1029/2026MS005795

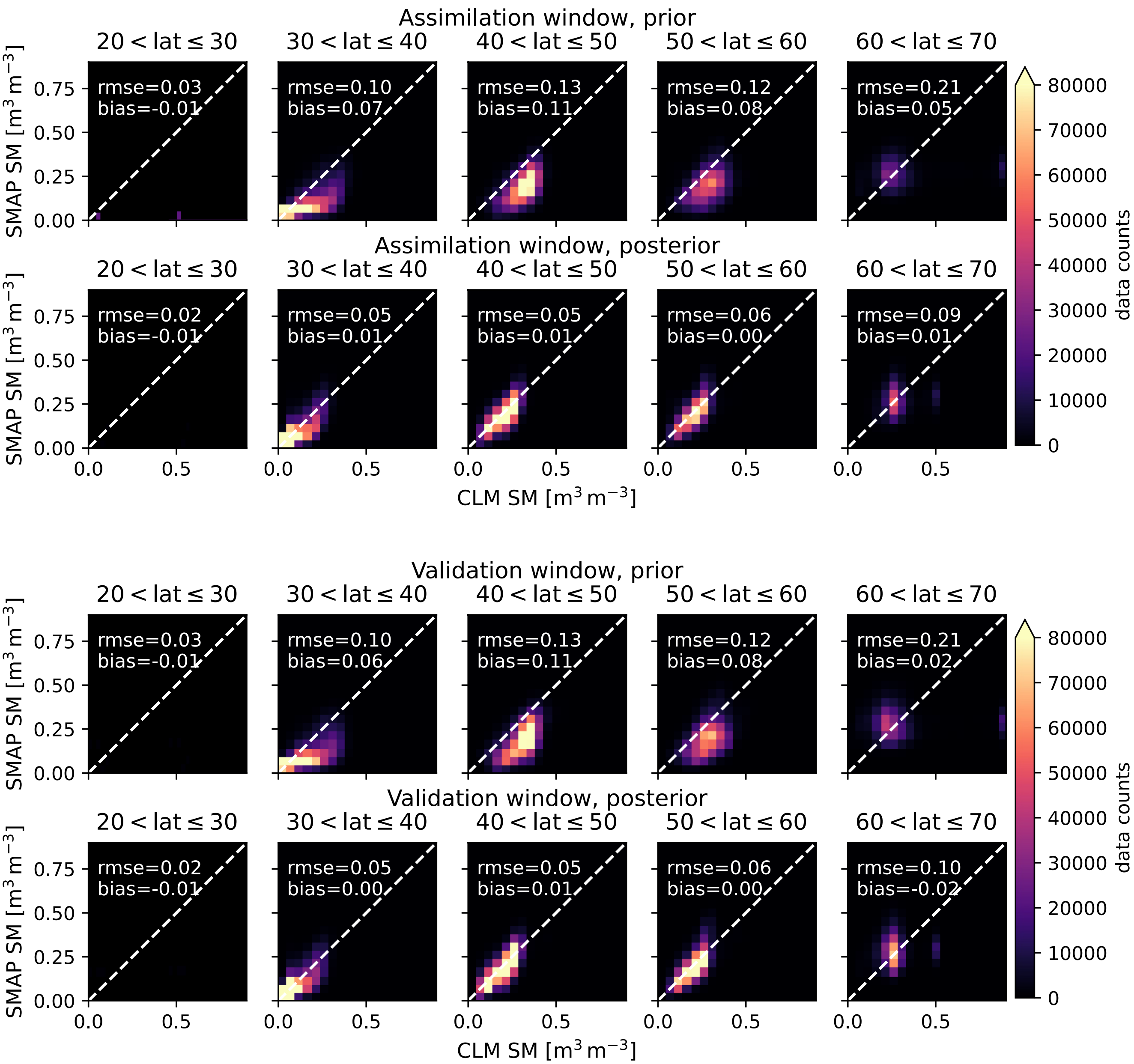

Figure 5. Density plots of modeled soil moisture values versus SMAP soil moisture retrievals. Results for the assimilation window are presented in the upper panel, results for the validation window in the lower panel. Each column represents a given latitude band, the upper row of each panel shows results for the prior model parameters, and the lower row of each panel shows the results after 5 iterations of the ES-MDA algorithm.

generally leading to wetter soil columns, but at the same time lower surface layer saturation and lower soil evaporation (Lawrence & Slater, 2008).

The high porosity of the organic soil is clearly visible for the high latitudes when looking at the prior model results of the surface soil moisture, for which three snapshots are presented in Figure 7. In these three snapshots the ground has started to thaw between 60°N and 70°N, resulting in very high volumetric soil moisture levels near the specified saturated water content of organic soil in CLM5 (around 0.9 $cm^3\ cm^{-3}$, Lawrence and Slater (2008)).

These high soil moisture levels are substantially decreased when looking at the posterior model results in Figure 7. There are several changes in the posterior parameter values leading to this difference, which will be discussed in more detail in Section 3.5: the overall contribution of organic soil with respect to mineral soil is decreased (through an increase in the parameter $\rho_{sc,\max}$), the porosity of organic soil is decreased ($\theta_{s,om}$), and the fraction of

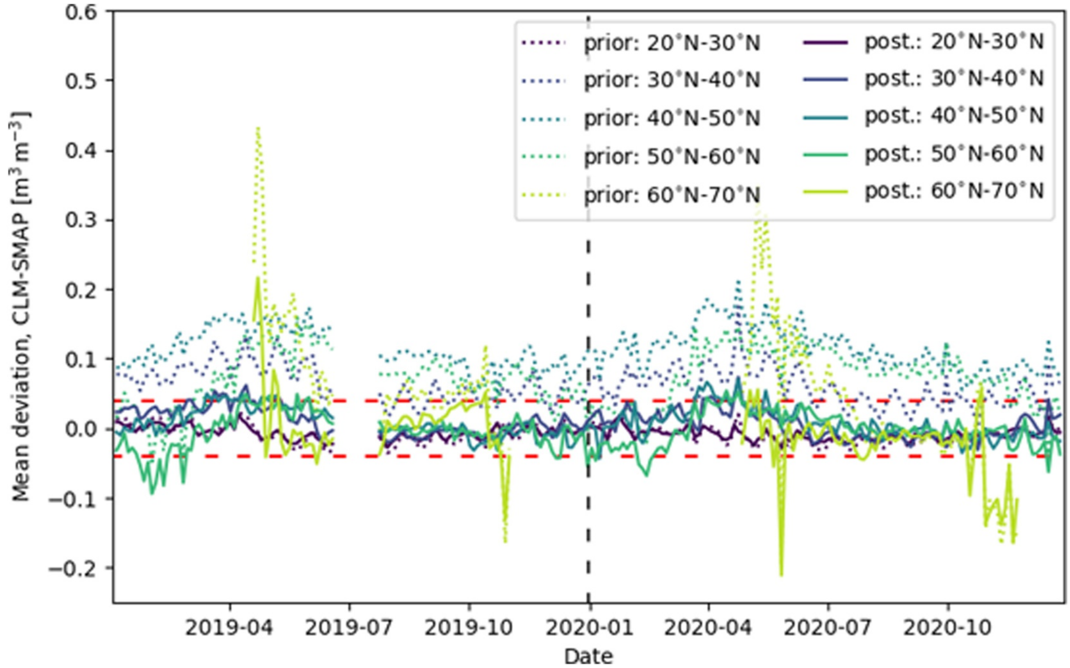

Figure 6. Time series for the mean SMAP-CLM mismatch over various latitude bands. Results for the prior model run are presented using the dotted lines, posterior model results after assimilating SMAP and ICOS data using the solid lines. Each color represents a different latitude band. The vertical black dashed line represents the date separating the assimilation and validation windows. As a reference, the target SMAP standard deviation (± 0.04 cm^3 cm^{-3}) is plotted using the horizontal red dashed lines.

soil carbon content between 60°N—70°N and 40°E—60°E is decreased. The posterior surface soil moisture during the thawing season for the high latitudes at around 0.5 cm^3 cm^{-3} is still somewhat higher than the SMAP soil moisture retrievals (see also the cluster of points to the right of the 1:1 line in Figure 5), but this could also be related to limitations of the soil moisture retrievals as discussed earlier.

As could be seen in Figure 4, the Nordic countries generally show a dry bias in the prior model run, with slight improvements in the posterior model run. This might also be related to the high soil carbon content, where an efficient transport of water down into the column and a low suction of organic soil can lead to a low surface layer saturation (Lawrence & Slater, 2008). The slight improvements in terms of an increased volumetric soil moisture can be attributed to the decreased contribution of organic soil with respect to mineral soil in the posterior model run (through the increase in the parameter $\rho_{sc,\max}$).

3.3. Evapotranspiration

While we have an overall improvement in the RMSE of the modeled evapotranspiration when using 5 iterations (See Figure 2), these improvements are not consistent over the entire domain and for every plant functional type.

In Figure 8 we present the RMSE between the modeled and the observed ICOS evapotranspiration estimates over our domain, with in the left panel the results as given for the prior model parameters. For most of the sites the RMSE lies below 1 mm d^{-1}, with especially high accuracies for Nordic needleleaf forests around 0.5 mm d^{-1}. In the right panel we show the decrease or increase in RMSE after the data assimilation. We find a few stations with a substantial decrease in RMSE, mainly a number of cropland and grassland sites in Germany and France. Many stations have little change in the RMSE, with changes between −0.1 and 0.1 mm d^{-1}. The Bosca Fontana station in Italy (IT-BFt) has a substantial increase in the RMSE of 0.25 mm d^{-1}, with Deciduous Broadleaf Forests as its dominant landcover. Other Deciduous Broadleaf Forest flux tower sites (DE-Hai, DE-HoH, DE-Hzd, FR-Hes) show varying levels of change in RMSE (ΔRMSE = −0.41, 0.00, 0.05, 0.19 mm d^{-1} respectively). This could suggest that representing deciduous broadleaf forests over our domain using one single plant functional type is insufficient.

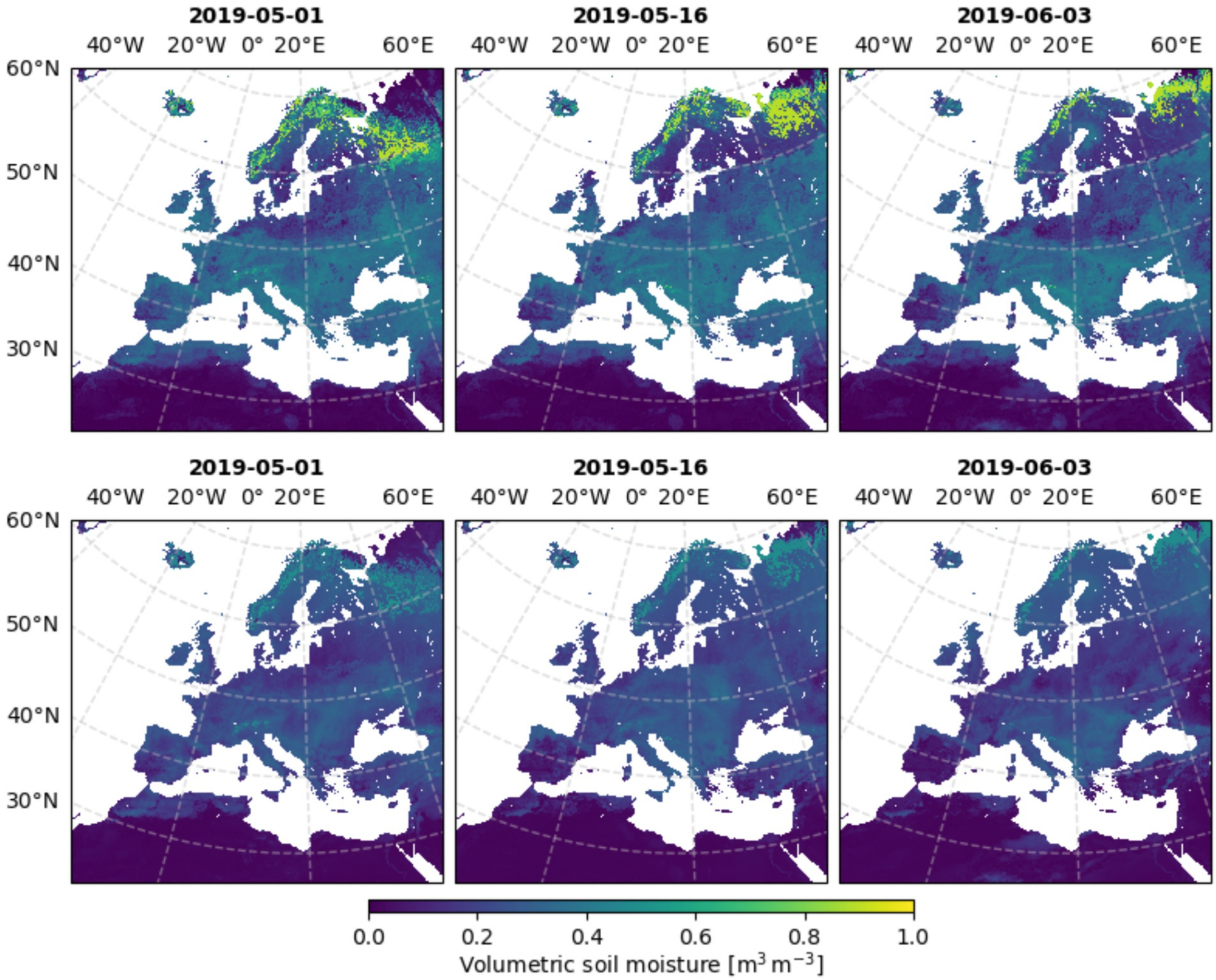

Figure 7. Snapshots of the modeled surface soil moisture for May-June 2019. Upper row: results for the prior parameter values. Lower row: results for the posterior parameter values. The surface soil moisture is calculated by taking the average liquid volumetric soil moisture of the two upper-most vertical layers (upper 6 cm).

Evapotranspiration correlation plots are presented in Figure 9. For some sites, such as mixed forests, grasslands, savannahs, we can observe an increase in performance for both the assimilation window and for the validation window. For other sites, such as woody savannahs and open shrublands the improvement in the assimilation window does not hold for the validation window. This could be caused by a lack of data, as well as the generally high variance of the data, given that only one site is present in the data set for both of these plant functional types (see also Figure 1). The model parameters could furthermore be calibrated for the particular climatological conditions during the year 2019. Repeating this analysis over longer time windows is required to see if parameters can be found that are universally valid under different atmospheric forcings.

It is important to stress the high variance present in the evapotranspiration data from the ICOS sites. In Section S2 of the Supporting Information S1 we took all ICOS evapotranspiration data pairs valid on the same day within 12.5 km of each other, to assess the variability of these evapotranspiration estimates at the length scale of the grid used in this work. We calculate a RMSE based on these observation pairs of 0.85 $\mathrm{mm\,d^{-1}}$, and a Pearson correlation coefficient of $R = 0.83$. This is close to the model-observation mismatch presented in Figure 9. This has the caveat that we get PFT specific evapotranspiration estimates from the model, whereas in the pairwise ICOS observation comparison the PFT sometimes differs between the pairs due to a lack of data. Nonetheless, this high variability within the in situ data should be considered for future model calibration studies. The variability appears to scale with the absolute amount of measured evapotranspiration, with most of the variability between the ICOS observation pairs around May to July.

10.1029/2026MS005795

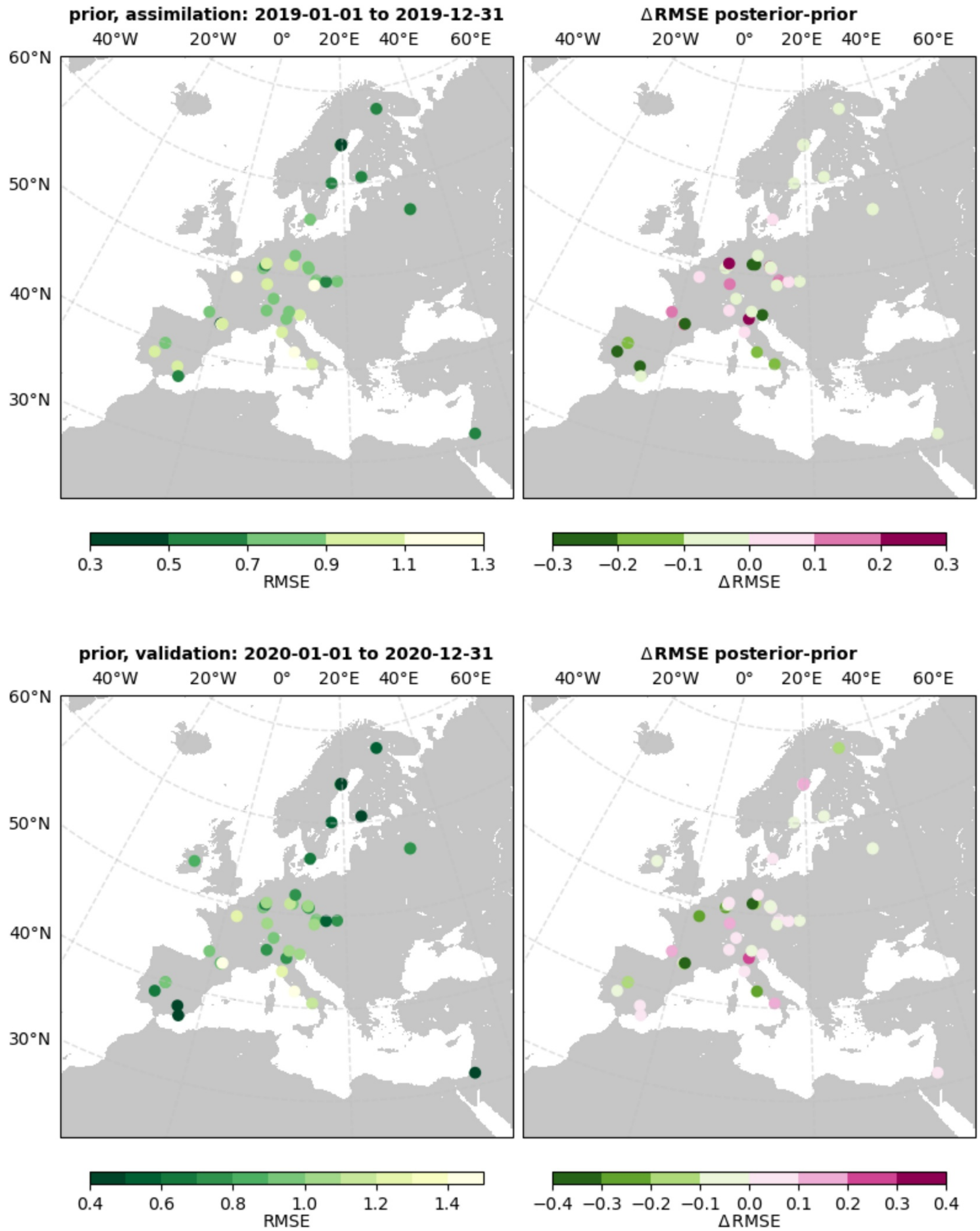

Figure 8. RMSE of modeled evapotranspiration versus observed evapotranspiration from ICOS sites (in mm d^{-1}). The left panels show the results for the prior model parameters, the right panels show the increase/decrease in RSME after the data assimilation. Results for the assimilation window are presented in the upper row, results for the validation window in the lower row.

3.4. Time Series Selected Sites

We show the soil moisture and evapotranspiration time series for two ICOS sites in Figures 10 and 11, which both show good improvement in the RMSE, and which both are covered by the observational data for the years 2019 and 2020. The first site is located in Germany (DE-Hai), with deciduous broadleaf forest as its dominant landcover, the second site is located in Spain (ES-LM1), with savannah as its dominant landcover. The rest of the 44 sites are presented in Section S8 of the Supporting Information S1. These two selected sites only serve as

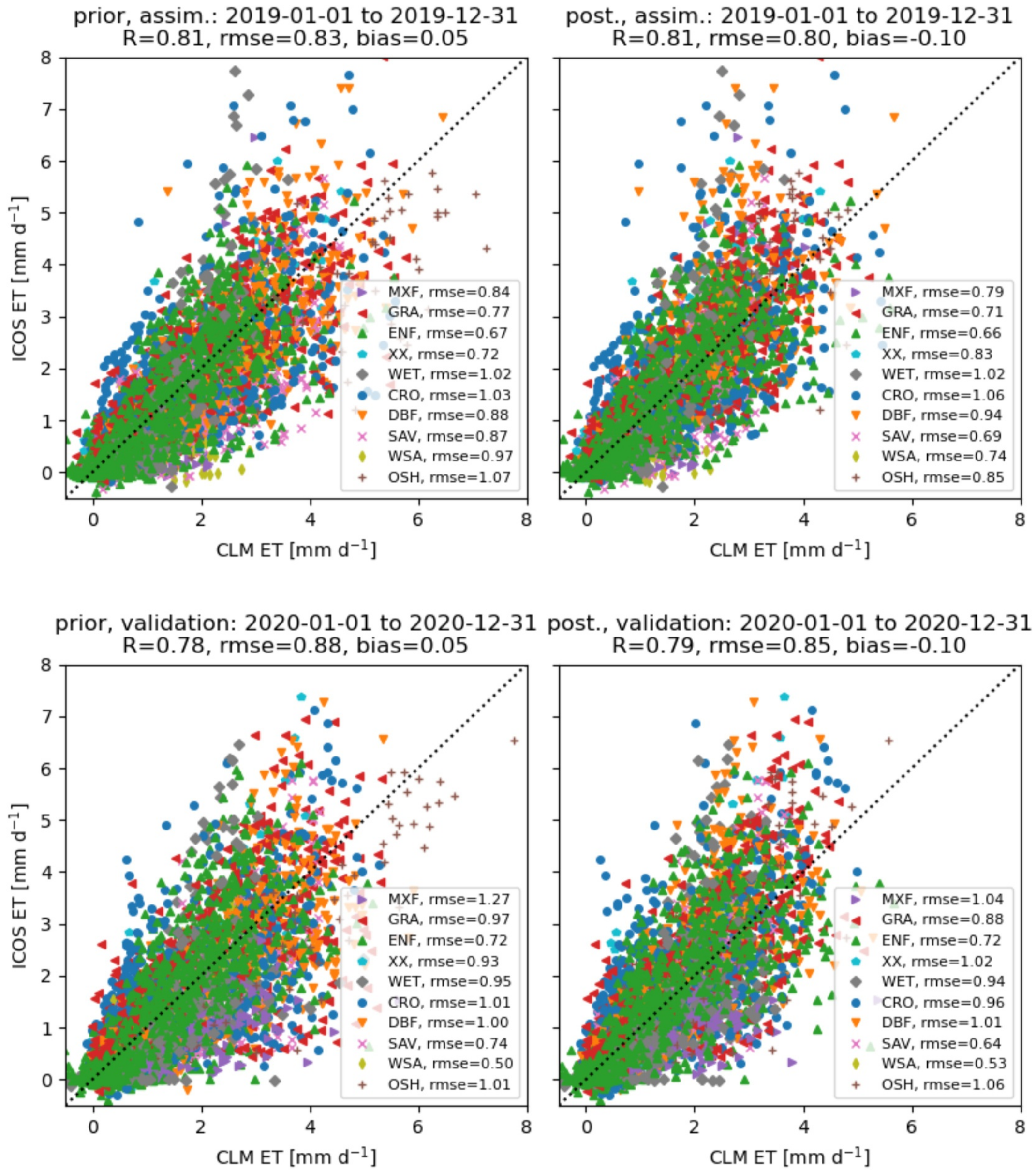

Figure 9. Correlation plots of modeled evapotranspiration versus observed evapotranspiration from ICOS sites. The left panels show the results for the prior model parameters, the right panels show the results for the posterior model parameters. Results for the assimilation window are presented in the upper row, results for the validation window in the lower row. The different symbols/colors indicate different landcover types.

examples where the data assimilation improved the results, to have a closer look at the dynamics and spread of the prior and posterior model runs.

For both sites we see that the SMAP soil moisture retrievals are reproduced well by the posterior model runs, with most of the observations intersecting with the posterior runs when considering the confidence interval. The posterior model performs better for both the assimilation and the validation windows. For all examples it is striking that the posterior ensemble shows very little spread for both the soil moisture and evapotranspiration. This is an issue that is encountered more often in the literature when applying ensemble smoothers and iterative ensemble smoothers (Emerick & Neto, 2023; Pinnington et al., 2021), and can be related to the relatively small ensemble size (64 members), which can lead to spurious correlations between the model parameters and observed state vectors, leading to an ensemble collapse.

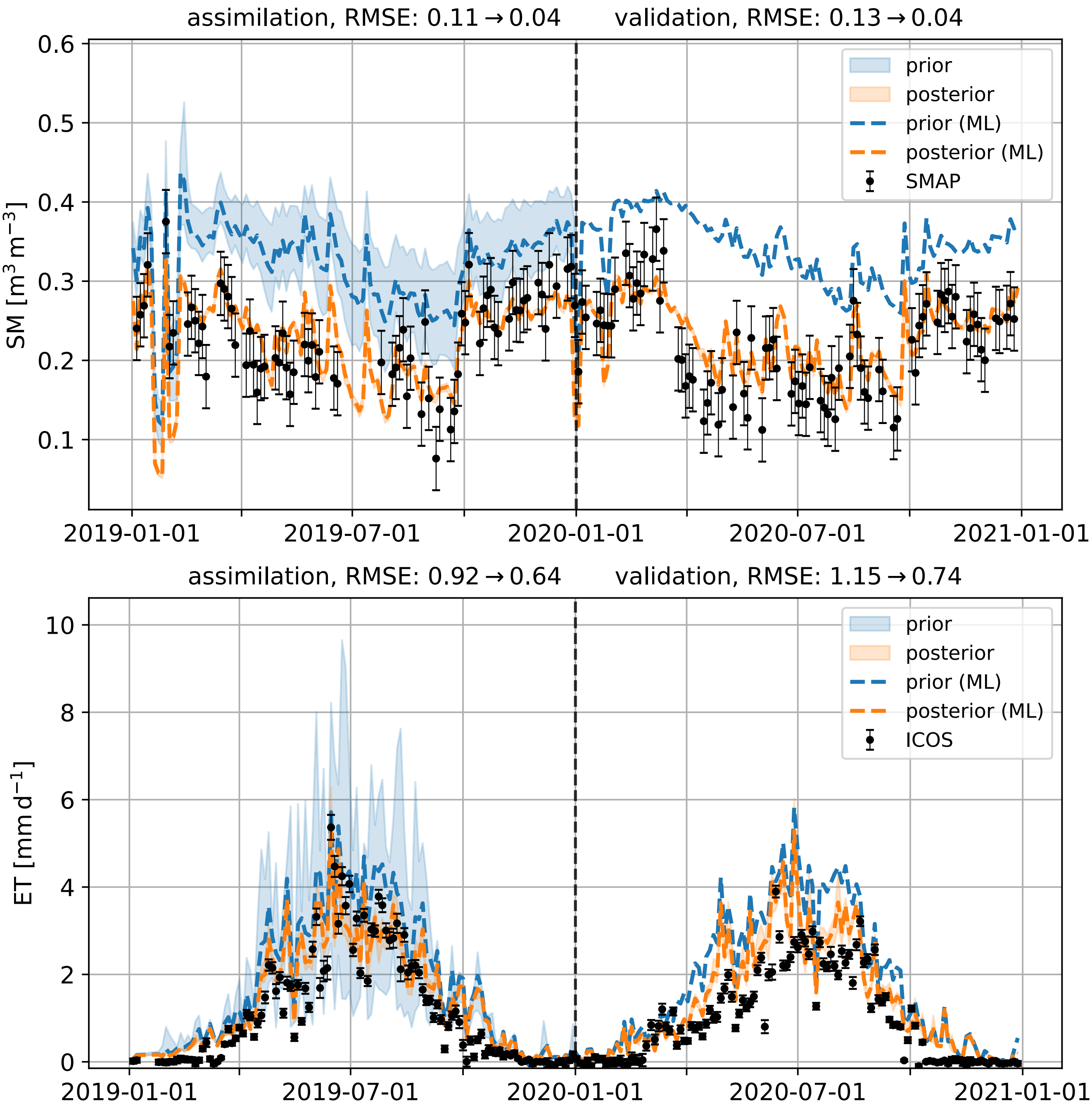

Figure 10. Comparison between CLM and SMAP/ICOS at the DE-Hai ICOS site (DBF). Upper panel: soil moisture time series. Lower panel: evapotranspiration time series. The ensemble spread is plotted using the blue and orange shading, model runs using the most likely (ML) parameter values are presented using the dashed blue and orange lines.

For the DE-Hai site, we can observe that the overall wet soil moisture bias is reduced. Additionally, we can observe an improvement in the dynamics on timescales in the order of days to weeks, with the magnitude of the increase in soil moisture just before/around October 2019 and October 2020 being captured more accurately in the posterior model. This is encouraging, as it could indicate that the updated parameters improve the dynamics of infiltration and runoff of water at the land surface. We can observe an overall decrease in the evapotranspiration error of the posterior model run, mainly due to reduced evapotranspiration around summer which follows the observed latent heat fluxes more accurately.

10.1029/2026MS005795

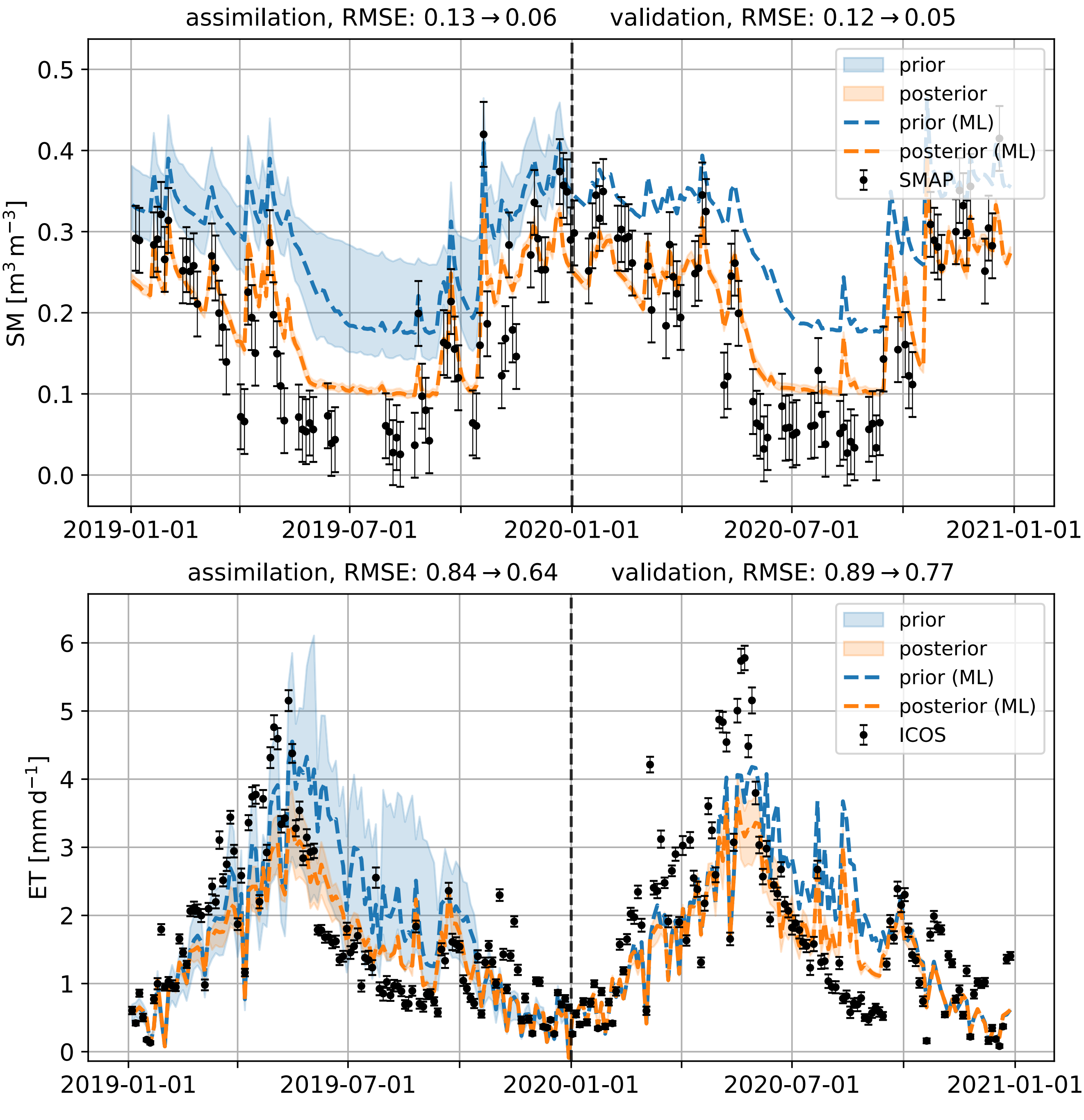

Figure 11. Comparison between CLM and SMAP/ICOS at the ES-LM1 ICOS site (SAV). Upper panel: soil moisture time series. Lower panel: evapotranspiration time series. The ensemble spread is plotted using the blue and orange shading, model runs using the most likely (ML) parameter values are presented using the dashed blue and orange lines.

For the ES-LM1 site, we can also observe an improvement in the soil moisture dynamics, although the model is still slightly more moist than the SMAP soil moisture retrievals in spring and summer. The rapid increase in soil moisture after October 2019 and October 2020 is captured well. For both years, the soil moisture remains relatively constant around June to August in both the model and the SMAP retrievals. The evapotranspiration slowly decays during these time periods, which is better captured by the posterior model. The posterior model fails to capture the more intense evapotranspiration events in spring, however, and the days with low evapotranspiration in the summer of 2020. Although the overall evapotranspiration error of the posterior model run is

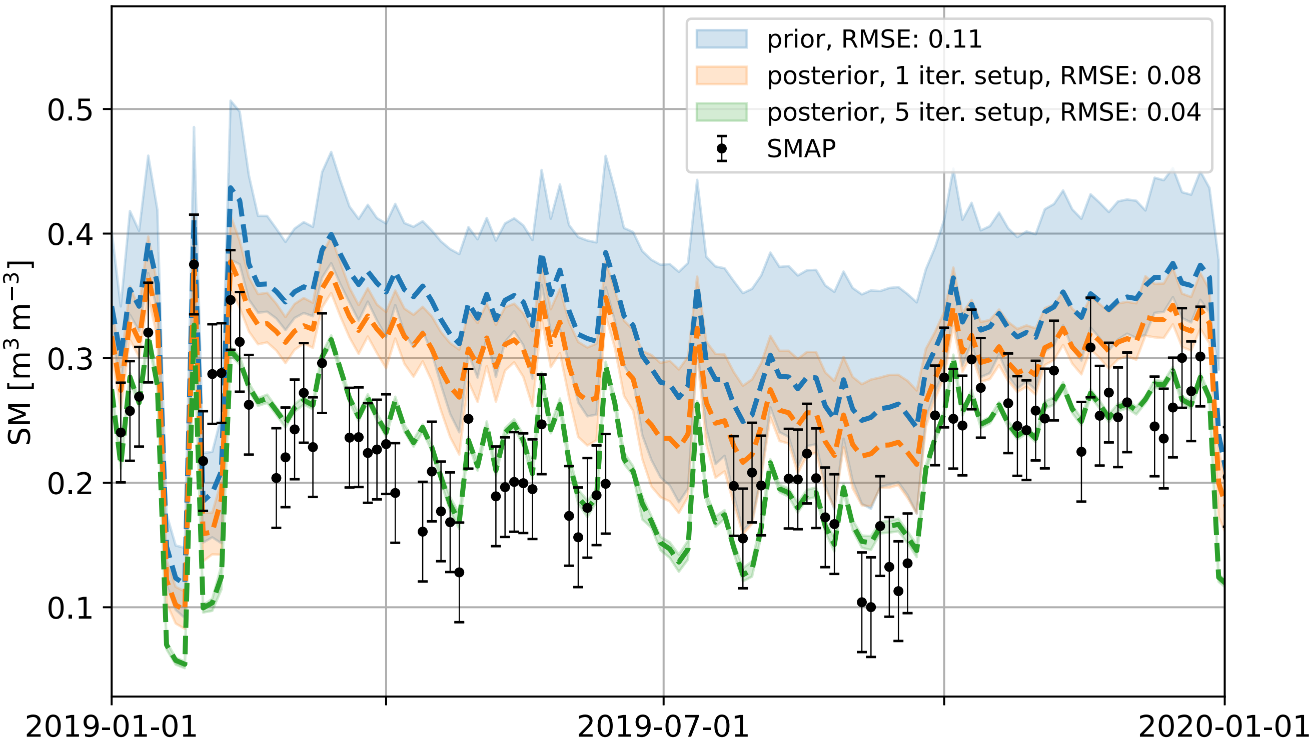

Figure 12. Example soil moisture timeseries resulting from the Ensemble Smoother (1 iteration) and the ES-MDA (5 iterations).

reduced, the more intense evapotranspiration events in spring are underpredicted, and variability within these months is missing. These issues could be related to the grid resolution being coarser than the ICOS flux tower footprints, or similarly related to the relatively coarse spatial and temporal resolution of the model forcing, resulting in missing subgrid-scale variability when comparing to the observations.

As noted earlier, the ES-MDA algorithm (Equation 6) is equivalent to running an Ensemble Smoother in the case of a linear forward solver (Emerick & Reynolds, 2012; Köpke et al., 2019). The multiple iterations used in the ES-MDA algorithm can help to reduce the impact of the linearization, that is applied in the standard Ensemble Smoother (Evensen et al., 2022). As shown in Figures 2 and 3, the improvements in modeled soil moisture are limited when using only one iteration of the ES-MDA algorithm, equivalent to running the standard Ensemble Smoother (Evensen et al., 2024). This can be explained due to the fact that our parameter-to-state mapping is relatively complex: the model parameters considered here are related in a non-trivial and likely non-linear way to the state variables (soil moisture and evapotranspiration). Where in more traditional data assimilation methods the model operator propagates the model states from an initial state to sequential states within the assimilation window, the situation presented here is arguably more complex, with a forward operator propagating a set of model parameters into model states within the assimilation window.

In Figure 12 we present a more detailed analysis for the case presented in Figure 10, focusing on soil moisture during the assimilation window. The ensemble range is presented for the prior parameter set, the 1-iteration ES-MDA setup, and the 5-iteration ES-MDA setup. As can be observed the modeled soil moisture for the prior parameter set has a wet bias, consistent with the general wet bias in Figure 3. The 1-iteration ES-MDA setup improves upon this wet bias, and for a large part of the year there is an overlap between the posterior distribution and the SMAP soil moisture retrieval data. The most likely parameter set still shows a wet bias, however. The 5-iteration ES-MDA setup largely removes the wet bias and fits most of the data points within their uncertainty intervals. The RMSE between the 1-iteration and 5-iteration ES-MDA setup is reduced from 0.08 to 0.04 for the assimilation window, and from 0.09 to 0.04 for the validation window (not shown here). As discussed before, however, the posterior distribution is underspread for the 5-iteration setup. We will further elaborate upon possible measures to resolve this issue in the conclusions and outlook, which includes, for example, different

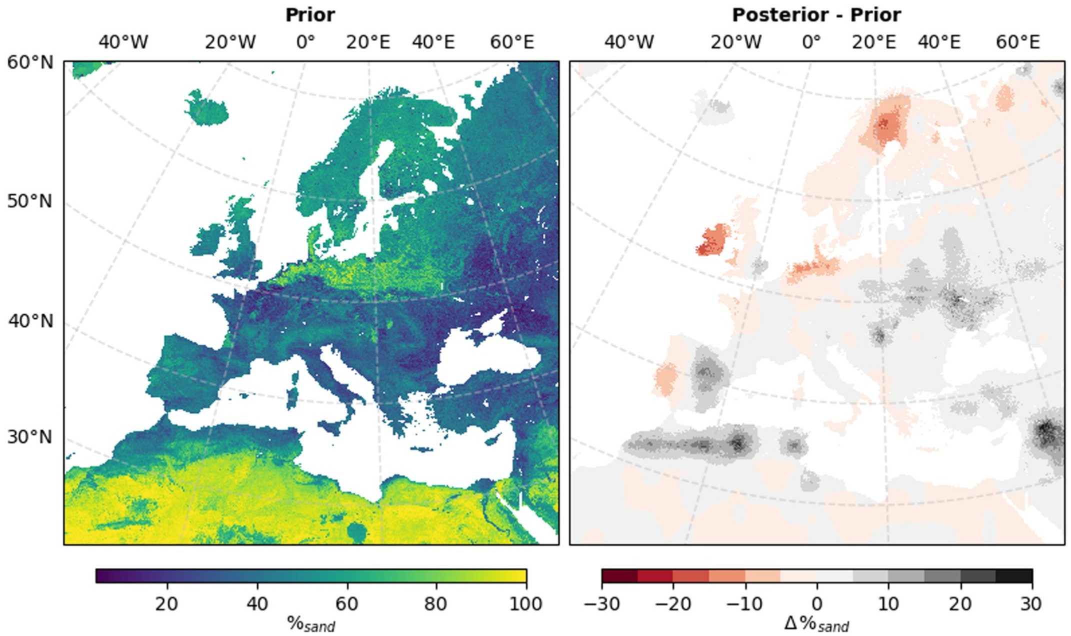

Figure 13. Percentage sand (most likely parameter values). Left panel: percentage sand used in the prior model run. Right panel: change in sand percentage after the assimilation.

inflation and localisation strategies (Silva et al., 2021), thinning of assimilated data (Emerick & Neto, 2023), or adding model bias terms to the smoother algorithm (Evensen, 2019).

3.5. Prior and Posterior Parameter Values

We present a brief overview of the prior and posterior model parameters, starting with parameters related to the soil hydrology.

The percentage of sand in the prior model, and the change in sand percentage for the posterior model is presented in Figure 13, both taking the most likely parameter values of the ensemble over the domain. Similary, the prior and posterior clay percentage and soil carbon content over the domain are presented in Figures 14 and 15, respectively.

Generally, we can observe increased sand percentages and decreased clay percentages in areas that are too wet in the prior model run. This includes several regions bordering the Mediterranean Sea around Spain, Morocco, Algeria, Tunisia, Lebanon and Syria, and regions north of the Black Sea around Ukraine. On the other hand, we can find decreased sand percentages and increased clay percentages in areas that are too dry in the prior model runs (see Figure 4). This includes the Nordic regions close to 70°N, the island of Ireland, the Netherlands, and north-west Germany. Increasing the sand percentage increases the hydraulic conductivity and reduces the soil suction in the pedotransfer functions (see Section S1 in Supporting Information S1), promoting a decreased top layer soil moisture. Additionally, increasing the sand percentage decreases the porosity of the soil, decreasing the capacity of the soil to hold water.

Changes in the soil carbon content are mainly visible in the high latitudes, where the decreased soil carbon content reduces the large wet bias as discussed earlier in relation to Figure 7, which can largely be attributed to a decreased porosity of the soil. Important to note here is that these large changes in soil carbon content are only present in areas where soil moisture observations are available. The more densely forested areas for which no SMAP retrievals were used could have similar high wet biases in the high latitudes. While the inclusion of global parameters in this study could theoretically improve soil moisture estimates in areas where no direct observations are available, it would be beneficial to include high-quality in situ observations of soil moisture in these regions for calibration of localized parameters such as soil texture. We will further elaborate upon this in the conclusions and discussions section.

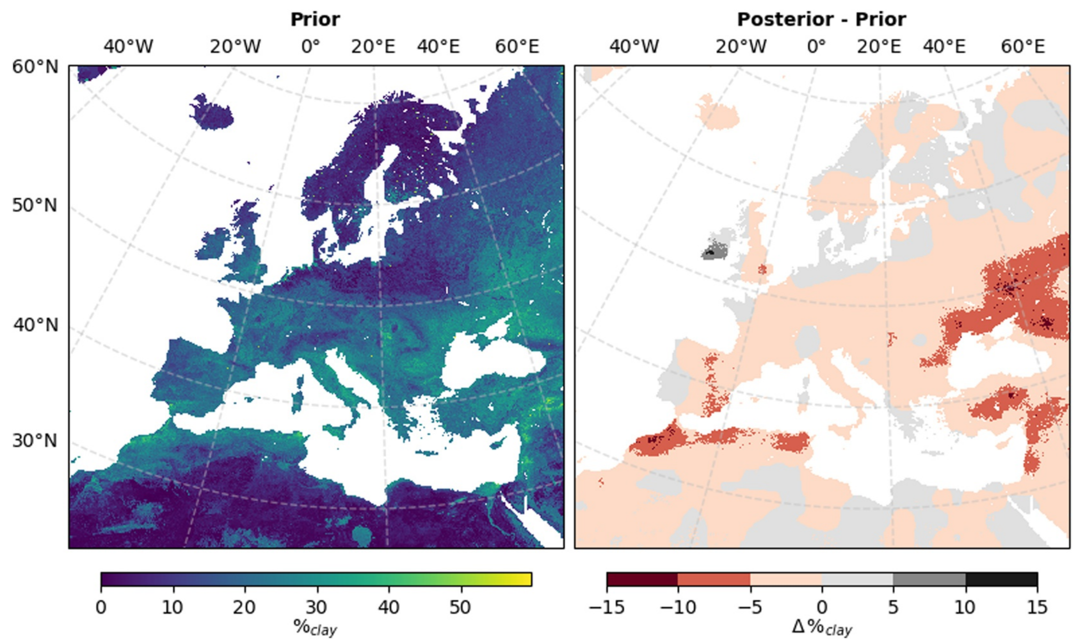

Figure 14. Percentage clay (most likely parameter values). Left panel: percentage clay used in the prior model run. Right panel: change in clay percentage after the assimilation.

Soil water characteristic curves, showing the soil matric potential given a certain soil water content θ, are plotted in Figure 16 for the prior model parameters (left panel) and the posterior model parameters (right panel). The soil matric potential is at its lowest strength near saturation, and is capped at -10^7 centimeters for the pedotransfer functions in CLM5. It is clearly visible that the soil matric properties are homogenized for the different types of soil after the parameter estimation process. The influence of clay on the soil matric potential is strongly decreased compared to the prior model parameters, with a much lower suction for soils dominated by clay content given the

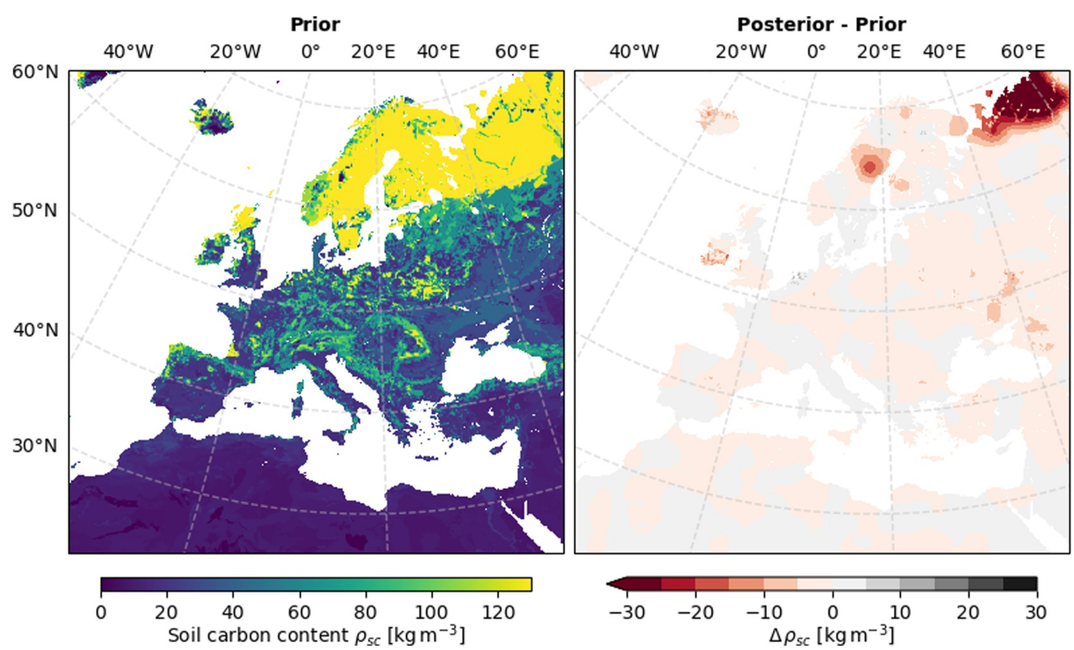

Figure 15. Soil carbon content (most likely parameter values). Left panel: soil carbon content used in the prior model run. Right panel: change in soil carbon content after the assimilation.

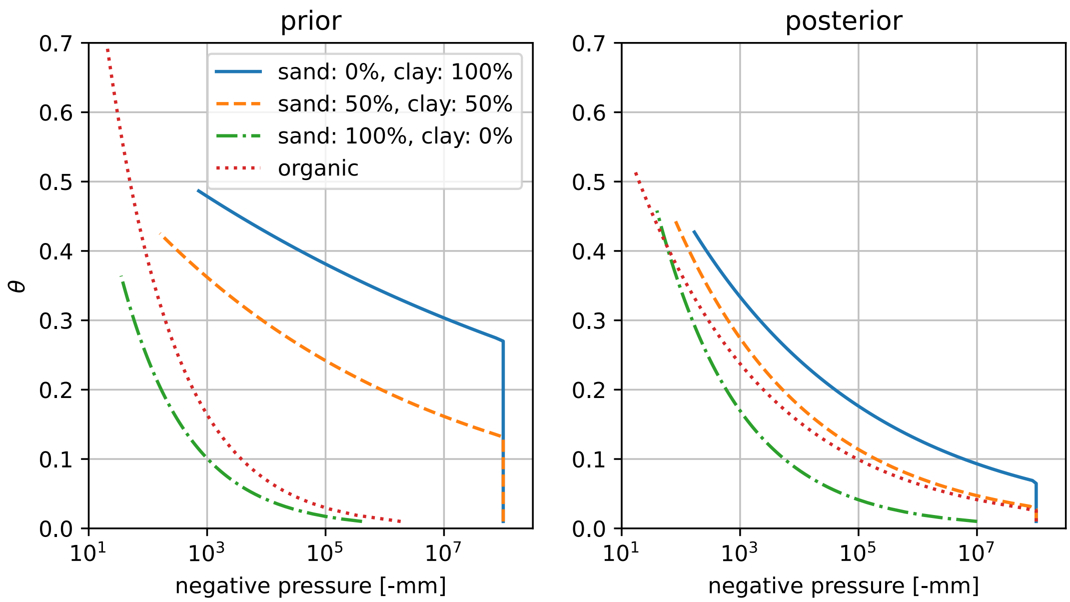

Figure 16. Soil water characteristic curves corresponding to the prior and posterior model runs. The soil matric potential (mm) is plotted against the soil water content θ for four example soil types: pure sand with no organic content (solid blue line), a mixture of 50% sand and 50% clay with no organic content (dashed orange line), pure clay with no organic content (dash-dotted green line), and purely organic soil (dashed red line).

same soil water content. On the other hand, the soil matric potential is slightly increased for soils dominated by sand and for organic soils.

The prior and posterior distributions for the underlying pedotransfer function parameters are presented in Figure S12 of the Supporting Information S1. One can see that homogenization of the soil water characteristic curves is introduced by a decrease in magnitude of the intercept and slope parameters for porosity ($\alpha_{\theta_s,miner.}$, $\beta_{\theta_s,miner.}$). This is generally consistent across the different configurations using a different number of iterations of the ES-MDA algorithm, although updates tend to be stronger when using more iterations. A similar decrease in magnitude can be seen for the intercept and slope parameters for the saturated hydraulic conductivity ($\alpha_{k_s,miner.}$, $\beta_{k_s,miner.}$). We can observe a consistent decrease in the $f_{sat,decay}$ parameter, which was observed to have a strong effect on the modeled soil water content in CLM5 (Yan et al., 2023a). This parameter increases surface runoff in the model, leading to an overall reduction of the wet model bias over our domain.

The homogenization of the soil water characteristic curves could be caused by different underlying factors, which require further study. One possibility is that the updated pedotransfer function parameters are compensating for other model errors. For example, inaccurate soil texture maps could lead to incorrect soil type fractions in the model gridpoints, leading to outliers in soil moisture. The homogenization of the soil hydraulic properties could lead to a decrease in these kind of outliers. Similarly, it could compensate for outliers that are introduced by inaccuracies in the SMAP retrievals for particular soil texture types. Other factors could be significant influences of subgrid-scale effects (Boone & Wetzel, 1999), or possible scale-dependence of parameters (Nykanen & Foufoula-Georgiou, 2001): soil texture properties measured under laboratory conditions do not necessarily lead to the correct results when applied at a kilometer-scale. We find that the global parameters governing soil hydraulic properties play a dominant role in reducing soil moisture RMSE and wet model bias. Density plots illustrating the mismatch between modeled soil moisture and SMAP retrievals are provided in Figures S8–S10 of the Supporting Information S1 for three configurations: (a) only global parameters active, (b) only soil texture perturbations active, and (c) both parameter sets active. Because the global parameters control the homogenization of soil matric properties (Figure 16), their adjustment tends to dampen the influence of local soil texture variations. As a result, in the configuration considered here, soil texture perturbations likely contribute to local fine-tuning primarily, rather than to large-scale improvements in model performance.

A comprehensive overview of all prior and posterior model parameters across different setups with varying numbers of ES-MDA iterations is provided in Section S6 of the Supporting Information S1. For certain parameters, such as soil texture, the updates show consistency, albeit with varying magnitudes. In general, more iterations of the ES-MDA algorithm result in stronger updates and reduced posterior parameter spread. However, one limitation of the parameter estimation approach presented here is the non-uniqueness of the solutions. Multiple parameter sets may produce similar effects on soil moisture and/or evapotranspiration, complicating the interpretation. This is particularly evident for PFT-specific parameters related to stomatal conductance and plant segment hydraulic conductivity, where no clear convergence to specific values is observed across the different setups.

For each PFT, we included parameters governing stomatal conductance (α_{g_s}, β_{g_s}) and plant segment hydraulic conductance ($k_{\max}$), as these parameters have been shown to significantly influence evapotranspiration in CLM5 (Dagon et al., 2020). However, the assimilated evapotranspiration data is likely too sparse and noisy to constrain all different parameters effectively. Variations in these conductance parameters can result in similar transformations of root soil moisture into latent heat fluxes. For example, in PFTs 3, 5, 6, 7, and 9, we observe a decrease in $k_{\max}$ after five ES-MDA iterations, but at the same time an increase in the stomatal conductance parameters α_{g_s} and/or β_{g_s}. Further research is required to find effective methods to deal with this issue, such as setting stricter prior constraints, or by using dimensionality reduction techniques to group parameters with similar effects on observed variables like evapotranspiration. For photosynthesis-related parameters, no clear trends emerge between prior and posterior values across the different ES-MDA setups, except for a tendency to increase J_{maxb0}. Running CLM5 with the biogeochemistry (BGC) module activated could help better constrain these parameters by allowing additional assimilation of Leaf Area Index (LAI) data and other biotic variables.

As noted earlier, the sparse and noisy ICOS evapotranspiration estimates limit the ability to constrain vegetation parameters. This is evident from the calculated RMSE of 0.85 mm, d^{-1} between ICOS observation pairs located within 12.5 km of each other. Meanwhile, the prior evapotranspiration estimates from CLM are nearly bias-free, with an error of just 0.05 mm, d^{-1}. As a result, little improvement can be made in this respect on large spatio-temporal scales by varying the vegetation parameters. When looking at Figure 9 we see no evidence of overfitting of the data, which would manifest as reduced errors during the assimilation window but increased errors during the validation window. This suggests that introducing more degrees of freedom in future studies could be beneficial. Possible approaches include refining the grid resolution, more elaborate handling of the flux tower footprints, or by introducing more flexibility in the system by allowing landcover and LAI maps to vary as an example.

4. Conclusions and Outlook

In this study, we explored the application of iterative ensemble smoothers in land surface models to enhance the accuracy of soil moisture and evapotranspiration simulations. Using the Ensemble Smoother with Multiple Data Assimilation (ES-MDA) algorithm (Emerick, 2016), we calibrated hydrological and ecosystem parameters, achieving a closer alignment with Soil Moisture Active Passive (SMAP) retrievals and ICOS flux tower evapotranspiration estimates compared to the baseline model. These improvements are evident during the observation assimilation period and, importantly, persist into the validation period, which extends up to 1 year beyond the assimilation window. Our findings highlight the advantage of employing multiple ES-MDA iterations over standard single-iteration Ensemble Smoother formulations. Multiple iterations enable better handling of the non-linear relationships between hydrological and ecosystem parameters and the observed variables, resulting in an improved fit to observational data. Post-assimilation, the model shows a much closer match to observed soil moisture, with localized adjustments driven by changes in soil texture and broader improvements across the model domain due to updates to hydrological and pedotransfer function parameters. In contrast, improvements in evapotranspiration are less pronounced. This is likely due to the sparse and noisy nature of the observed evapotranspiration data and the fact that the prior modeled evapotranspiration was already relatively bias-free. Despite this, the results demonstrate the potential of iterative ensemble smoothers to refine parameter estimates and improve land surface model performance. The simultaneous assimilation of SMAP and ICOS data yields promising results, as model biases after three to five iterations are notably reduced. Future studies would benefit from improved spatial coverage of evapotranspiration observations to better identify potential synergies between the two data sources. In addition, assimilating further atmospheric and near-surface variables, such as 2-m relative humidity, could strengthen the coupling between land–atmosphere fluxes and land surface processes.

Further investigations into getting a better representation of the posterior model variance are required. A number of schemes have been published in the literature that could counteract the loss of posterior ensemble variance, where some recent studies suggested that singular value truncation (Evensen & Eikrem, 2018), or using more sophisticated schemes to tune the inflation factors α can help (Silva et al., 2021). In addition, future work should examine the impact of thinning the assimilated observations (Emerick & Neto, 2023), as the dense spatial and temporal sampling of soil moisture retrievals, combined with neglected observation error covariances, may promote overfitting and lead to an artificial reduction of ensemble spread. Related land surface modeling studies using SMAP data to calibrate pedotransfer function parameters also found narrow posterior parameter distributions, suggesting that ensemble inflation might be necessary (Pinnington et al., 2021). A further promising direction is the adoption of a weak-constraint formulation of the ensemble smoother, in which model error terms are estimated jointly with model parameters. Such approaches relax the perfect-model assumption and explicitly account for model inadequacy, and have been shown to mitigate underestimation of posterior uncertainty in iterative ensemble smoothers (Evensen, 2019). Importantly, further investigations are required to assess the effect of uncertainties in the model forcing data. It would be possible to use the ERA5 ensemble product (Hersbach et al., 2020) to apply perturbed atmospheric forcings to individual ES-MDA ensemble members, thereby accounting for forcing uncertainties, for example, in precipitation (Lavers et al., 2022).

Improvement in the modeled evapotranspiration when comparing to the flux tower sites is not always consistent over our domain. As an example, there are differences in improvement/degradation for flux tower sites located in deciduous broadleaf forests (DBF). One solution might be to introduce more PFT's, for example, accounting for differences in iso/anisohydric behavior in plants (Hwang et al., 2017; Wu et al., 2021), which could explain why in our case there is a degraded performance for DBF sites over France and Italy, but mainly an improvement for DBF sites over Germany. Instead, one could also consider specifying the underlying effective parameters (e.g., stomatal conductance, plant segment hydraulic conductivity) directly at the grid-level, instead of having to keep introducing additional discrete PFT's.

Some areas of our domain are lacking observational data, such as the densely vegetated areas in the higher latitudes (around 60°N) where no SMAP soil moisture retrievals were available. We recommend gathering more in situ observations of soil moisture for these areas in follow-up data assimilation studies. As observed for the Russian tundra, the model shows a substantial mismatch with respect to the SMAP soil moisture retrievals in the thawing season. These mismatches are greatly reduced for the posterior model parameters, as the iterative ensemble smoother decreases the soil carbon content, and thus reduces the soil porosity. However, similar issues might be present in other areas not covered by SMAP, in which case in situ data of soil moisture might help, but also remotely sensed land surface temperature and snow cover observations to accurately capture the exact timing of the freezing and thawing cycles. In data-sparse areas where satellite observations of soil moisture are not feasible and in situ data should be used instead, further optimization of the localisation radius should be considered: where updates in data-rich areas to parameters can be kept local, it is likely beneficial to increase the localisation radius in data-sparse regions.

The parameters estimated here may compensate not only for uncertainties in the forcing data and errors in other, unestimated parameters, but also for structural deficiencies in the model, including temporal variations that are not explicitly represented in the model formulation. As a result, the calibrated parameters should be interpreted as effective parameters rather than strictly physical constants. Although the ERA5 data set generally shows high correlation with gauge-based precipitation over Europe, it has a documented slight wet bias on average (around $0.2\ \mathrm{mm\,d^{-1}}$, Lavers et al., 2022). For most locations and most months this should be less than 10% of the mean precipitation (see Section S7 in Supporting Information S1), but this can still have significant impacts on the estimated parameter values. This work forms part of a broader investigation into data assimilation in coupled atmospheric and land surface models. In future studies we plan to extend this framework to a coupled system with CLM5 and the Icosahedral Nonhydrostatic (ICON) model (Zängl et al., 2015), where we will further consider improving predicted precipitation patterns.

Effective parameters may also compensate for limitations in the land surface model itself. The updated soil texture should therefore not be interpreted as a more faithful representation of reality, as the optimized values depend on the specific model formulation and, in the case of a complex model such as CLM5, on which model components are activated during the simulation. The Cosby parameterizations used for the CLM5 pedotransfer functions are relatively simplistic, as mineral soil hydraulic properties are described using univariate relationships (Equations 1–4). Employing more realistic multivariate pedotransfer functions, potentially including additional soil constituents such as loam, could therefore lead to substantially different optimized soil texture maps. Finally, parameters treated as time-invariant during calibration may implicitly compensate for processes that vary seasonally or are structurally missing from the model. For example, plant hydraulic properties have been shown to exhibit seasonal variability (Zhang et al., 2025), and soil hydraulic properties may vary seasonally due to changes in soil organic matter content (Li et al., 2024). Consequently, the time-invariant parameters estimated by ES-MDA should be interpreted as effective descriptors of model behavior over the calibration period.

Follow-up work could focus on evaluating the sensitivity of state vectors to the particular parameters, in order to identify which parameters influence the model mismatch in certain areas the most. This would possibly allow for thinning the model parameters, which could lead to more robust parameter estimates related to evapotranspiration, given the fact we see no clear convergence to particular values for plant functional type parameters. The use of surrogate models, such as Gaussian Process models (Bhattacharjee et al., 2019), could aid in extending the ES-MDA ensemble without increasing computational costs significantly. Running CLM5 with the biogeochemistry (BGC) module activated would allow us to assimilate additional data that could inform us on biological processes. In the current setup, climatological values are used for the Leaf Area Index (LAI). Instead, LAI could be determined prognostically with the BGC module activated, which could then be assimilated using, for example, MODIS LAI retrievals. Prognostically determined Gross Primary Production (GPP) could furthermore be compared to GPP observations from eddy covariance fluxes (Pinnington et al., 2020).

Conflict of Interest

The authors declare no conflicts of interest relevant to this study.

Availability Statement

The SMAP Enhanced L3 Radiometer product (version 9) used in this study is publicly available at https://doi.org/10.5067/NJ34TQ2LFE90 (O'Neill et al., 2020). The ICOS eddy covariance flux data are publicly available at https://doi.org/10.18160/2G60-ZHAK (Warm Winter 2020 Team and ICOS Ecosystem Thematic Centre, 2022).

The fork of version 5 of the Community Land Model (eCLM) used for running the land surface model is available without restrictions and developed openly at https://github.com/HPSCTerrSys/eCLM (HPSCTerrSys, 2024b); the version used in this study is archived at https://doi.org/10.5281/zenodo.19912983 (Kaandorp, 2026a). The software developed for this manuscript, including the data assimilation framework and the Jupyter Notebooks used to create the figures, are archived at https://doi.org/10.5281/zenodo.19912810 (Kaandorp, 2026b).

Acknowledgments

This work was funded by the Deutsche Forschungsgemeinschaft (DFG, German Research Foundation) under project SFB 1502/1–2022—project number 450058266 (DETECT). The authors gratefully acknowledge the computing time granted on the supercomputer JUWELS at Forschungszentrum Jülich, and support through the Dragon 5 project. We would like to thank Dr. Johannes Keller for his help coordinating the JUWELS supercomputer resources. The authors thank the reviewers for their constructive feedback, which helped improve the manuscript. Open Access funding enabled and organized by Projekt DEAL.

References

Abdallah, M. B., Karray, F., Mhiri, N., Mei, N., Quéméneur, M., Cayol, J.-L., et al. (2016). Prokaryotic diversity in a Tunisian hypersaline lake, Chott El Jerid. *Extremophiles*, *20*(2), 125–138. https://doi.org/10.1007/s00792-015-0805-7

Ali, A. A., Xu, C., Rogers, A., Fisher, R. A., Wullschleger, S. D., Massoud, E. C., et al. (2016). A global scale mechanistic model of photosynthetic capacity (LUNA V1.0). *Geoscientific Model Development*, *9*(2), 587–606. https://doi.org/10.5194/gmd-9-587-2016

Allen, R. G. (Ed.). (2000). *Crop evapotranspiration: Guidelines for computing crop water requirements, Number 56 in FAO irrigation and drainage paper* (repr edition). Food and Agriculture Organization of the United Nations.

Aubinet, M., Vesala, T., & Papale, D. (Eds.). (2012). *Eddy covariance: A practical guide to measurement and data analysis*. Springer Atmospheric Sciences. Springer.

Bacour, C., MacBean, N., Chevallier, F., Léonard, S., Koffi, E. N., & Peylin, P. (2023). Assimilation of multiple datasets results in large differences in regional-to global-scale NEE and GPP budgets simulated by a terrestrial biosphere model. *Biogeosciences*, *20*(6), 1089–1111. https://doi.org/10.5194/bg-20-1089-2023

Baldocchi, D. D., Keeney, N., Rey-Sanchez, C., & Fisher, J. B. (2022). Atmospheric humidity deficits tell us how soil moisture deficits downregulate ecosystem evaporation. *Advances in Water Resources*, *159*, 104100. https://doi.org/10.1016/j.advwatres.2021.104100

Bartholome, E., & Belward, A. S. (2005). GLC2000: A new approach to global land cover mapping from Earth observation data. *International Journal of Remote Sensing*, *26*(9), 1959–1977. https://doi.org/10.1080/01431160412331291297

Bastrikov, V., MacBean, N., Bacour, C., Santaren, D., Kuppel, S., & Peylin, P. (2018). Land surface model parameter optimisation using in situ flux data: Comparison of gradient-based versus random search algorithms (a case study using ORCHIDEE v1.9.5.2). *Geoscientific Model Development*, *11*(12), 4739–4754. https://doi.org/10.5194/gmd-11-4739-2018

Belleflamme, A., Goergen, K., Wagner, N., Kollet, S., Bathiany, S., El Zohbi, J., et al. (2023). Hydrological forecasting at impact scale: The integrated ParFlow hydrological model at 0.6 km for climate resilient water resource management over Germany. *Frontiers in Water*, *5*, 1183642. https://doi.org/10.3389/frwa.2023.1183642

Bhattacharjee, N. V., Ranjan, P., Mandal, A., & Tollner, E. W. (2019). A history matching approach for calibrating hydrological models. *Environmental and Ecological Statistics*, *26*(1), 87–105. https://doi.org/10.1007/s10651-019-00420-9

Blunden, J., & Arndt, D. (2020). State of the climate in 2019. *Bulletin of the American Meteorological Society*, *101*(8), S1–S429. https://doi.org/10.1175/2020BAMSStateoftheClimate.1

Blunden, J., & Boyer, T. (2021). State of the climate in 2020. *Bulletin of the American Meteorological Society*, *102*(8), S1–S475. https://doi.org/10.1175/2021bamsstateoftheclimate.1

Boas, T., Bogena, H., Ryu, D., Western, A., & Hendricks Franssen, H.-J. (2024). Multi-decadal soil moisture and crop yield variability—A case study with the Community Land Model (CLM5). *Journal of Advances in Modeling Earth Systems*, *16*(9), e2023MS004023. https://doi.org/10.1029/2023ms004023

Boas, T., Bogena, H. R., Ryu, D., Vereecken, H., Western, A., & Hendricks Franssen, H.-J. (2023). Seasonal soil moisture and crop yield prediction with fifth-generation seasonal forecasting system (SEAS5) long-range meteorological forecasts in a land surface modelling approach. *Hydrology and Earth System Sciences*, *27*(16), 3143–3167. https://doi.org/10.5194/hess-27-3143-2023

Boone, A., & Wetzel, P. J. (1999). A simple scheme for modeling sub-grid soil texture variability for use in an atmospheric climate model. *Journal of the Meteorological Society of Japan. Series II*, *77*(1B), 317–333. https://doi.org/10.2151/jmsj1965.77.1b_317

Chen, Y., & Oliver, D. S. (2017). Localization and regularization for iterative ensemble smoothers. *Computational Geosciences*, *21*(1), 13–30. https://doi.org/10.1007/s10596-016-9599-7

Cheng, Y., Huang, M., Zhu, B., Bisht, G., Zhou, T., Liu, Y., et al. (2021). Validation of the community land model version 5 over the contiguous United States (CONUS) using in situ and remote sensing data sets. *Journal of Geophysical Research: Atmospheres*, *126*(5), e2020JD033539. https://doi.org/10.1029/2020jd033539

Chu, H., Luo, X., Ouyang, Z., Chan, W. S., Dengel, S., Biraud, S. C., et al. (2021). Representativeness of Eddy-Covariance flux footprints for areas surrounding AmeriFlux sites. *Agricultural and Forest Meteorology*, *301–302*, 108350. https://doi.org/10.1016/j.agrformet.2021.108350

Clapp, R. B., & Hornberger, G. M. (1978). Empirical equations for some soil hydraulic properties. *Water Resources Research*, *14*(4), 601–604. https://doi.org/10.1029/wr014i004p00601

Copernicus Climate Change Service, Climate Data Store. (2018). Leaf area index and fraction absorbed of photosynthetically active radiation 10-daily gridded data from 1981 to present [Dataset]. *Copernicus Climate Change Service (C3S) Climate Data Store (CDS)*. https://doi.org/10.24381/cds.7e59b01a

Cosby, B. J., Hornberger, G. M., Clapp, R. B., & Ginn, T. R. (1984). A statistical exploration of the relationships of soil moisture characteristics to the physical properties of soils. *Water Resources Research*, *20*(6), 682–690. https://doi.org/10.1029/wr020i006p00682

Dagon, K., Sanderson, B. M., Fisher, R. A., & Lawrence, D. M. (2020). A machine learning approach to emulation and biophysical parameter estimation with the Community Land Model, version 5. *Advances in Statistical Climatology, Meteorology and Oceanography*, *6*(2), 223–244. https://doi.org/10.5194/ascmo-6-223-2020

Danabasoglu, G., Lamarque, J.-F., Bacmeister, J., Bailey, D. A., DuVivier, A. K., Edwards, J., et al. (2020). The Community Earth System Model Version 2 (CESM2). *Journal of Advances in Modeling Earth Systems*, *12*(2), e2019MS001916. https://doi.org/10.1029/2019ms001916

De Lannoy, G. J. M., Bechtold, M., Albergel, C., Brocca, L., Calvet, J.-C., Carrassi, A., et al. (2022). Perspective on satellite-based land data assimilation to estimate water cycle components in an era of advanced data availability and model sophistication. *Frontiers in Water*, *4*, 981745. https://doi.org/10.3389/frwa.2022.981745

Dharssi, I., Bovis, K. J., Macpherson, B., & Jones, C. P. (2011). Operational assimilation of ASCAT surface soil wetness at the Met Office. *Hydrology and Earth System Sciences*, *15*(8), 2729–2746. https://doi.org/10.5194/hess-15-2729-2011

Dolman, A. J., Miralles, D. G., & de Jeu, R. A. (2014). Fifty years since Monteith's 1965 seminal paper: The emergence of global ecohydrology. *Ecohydrology*, *7*(3), 897–902. https://doi.org/10.1002/eco.1505

Emerick, A. A. (2016). Analysis of the performance of ensemble-based assimilation of production and seismic data. *Journal of Petroleum Science and Engineering*, *139*, 219–239. https://doi.org/10.1016/j.petrol.2016.01.029

Emerick, A. A. (2019). Analysis of geometric selection of the data-error covariance inflation for ES-MDA. *Journal of Petroleum Science and Engineering*, *182*, 106168. https://doi.org/10.1016/j.petrol.2019.06.032

Emerick, A. A., & Neto, G. M. S. (2023). Investigation on the production data frequency for assimilation with ensemble smoother. *Geoenergy Science and Engineering*, *231*, 212356. https://doi.org/10.1016/j.geoen.2023.212356

Emerick, A. A., & Reynolds, A. C. (2012). History matching time-lapse seismic data using the ensemble Kalman filter with multiple data assimilations. *Computational Geosciences*, *16*(3), 639–659. https://doi.org/10.1007/s10596-012-9275-5

Emerick, A. A., & Reynolds, A. C. (2013). Ensemble smoother with multiple data assimilation. *Computers & Geosciences*, *55*, 3–15. https://doi.org/10.1016/j.cageo.2012.03.011

Entekhabi, D., Yueh, S., O'Neill, P., Kellogg, K., Allen, A., Bindlish, R., et al. (2014). SMAP handbook–soil moisture active passive: Mapping soil moisture and freeze/thaw from space.

Eshonkulov, R., Poyda, A., Ingwersen, J., Wizemann, H.-D., Weber, T. K. D., Kremer, P., et al. (2019). Evaluating multi-year, multi-site data on the energy balance closure of eddy-covariance flux measurements at cropland sites in southwestern Germany. *Biogeosciences*, *16*(2), 521–540. https://doi.org/10.5194/bg-16-521-2019

Evensen, G. (2019). Accounting for model errors in iterative ensemble smoothers. *Computational Geosciences*, *23*(4), 761–775. https://doi.org/10.1007/s10596-019-9819-z

Evensen, G., & Eikrem, K. S. (2018). Conditioning reservoir models on rate data using ensemble smoothers. *Computational Geosciences*, *22*(5), 1251–1270. https://doi.org/10.1007/s10596-018-9750-8

Evensen, G., Raanes, P. N., Stordal, A. S., & Hove, J. (2019). Efficient implementation of an iterative ensemble smoother for data assimilation and reservoir history matching. *Frontiers in Applied Mathematics and Statistics*, *5*, 47. https://doi.org/10.3389/fams.2019.00047

Evensen, G., & van Leeuwen, P. J. (2000). An ensemble Kalman smoother for nonlinear dynamics. *Monthly Weather Review*, *128*(6), 1852–1867. https://doi.org/10.1175/1520-0493(2000)128<1852:aeksfn>2.0.co;2

Evensen, G., Vossepoel, F. C., & Van Leeuwen, P. J. (2022). Data assimilation fundamentals: A unified formulation of the state and parameter estimation problem. In *Springer textbooks in Earth sciences, geography and environment*. Springer International Publishing.

Evensen, G., Vossepoel, F. C., & van Leeuwen, P. J. (2024). Iterative ensemble smoothers for data assimilation in coupled nonlinear multiscale models. *Monthly Weather Review*, *152*(6), 1277–1301. https://doi.org/10.1175/mwr-d-23-0239.1

Fisher, R. A., & Koven, C. D. (2020). Perspectives on the future of land surface models and the challenges of representing complex terrestrial systems. *Journal of Advances in Modeling Earth Systems*, *12*(4), e2018MS001453. https://doi.org/10.1029/2018ms001453

Franssen, H. H., Stöckli, R., Lehner, I., Rotenberg, E., & Seneviratne, S. (2010). Energy balance closure of eddy-covariance data: A multisite analysis for European FLUXNET stations. *Agricultural and Forest Meteorology*, *150*(12), 1553–1567. https://doi.org/10.1016/j.agrformet.2010.08.005

Franz, D., Acosta, M., Altimir, N., Arriga, N., Arrouays, D., Aubinet, M., et al. (2018). Towards long-term standardised carbon and greenhouse gas observations for monitoring Europe's terrestrial ecosystems: A review. *International Agrophysics*, *32*(4), 439–455. https://doi.org/10.1515/intag-2017-0039

Furusho-Percot, C., Goergen, K., Hartick, C., Kulkarni, K., Keune, J., & Kollet, S. (2019). Pan-European groundwater to atmosphere terrestrial systems climatology from a physically consistent simulation. *Scientific Data*, *6*(1), 320. https://doi.org/10.1038/s41597-019-0328-7

Gao, X., Avramov, A., Saikawa, E., & Schlosser, C. A. (2021). Emulation of Community Land Model version 5 (CLM5) to quantify sensitivity of soil moisture to uncertain parameters. *Journal of Hydrometeorology*, *22*(2), 259–278. https://doi.org/10.1175/jhm-d-20-0043.1

Gasper, F., Goergen, K., Shrestha, P., Sulis, M., Rihani, J., Geimer, M., & Kollet, S. (2014). Implementation and scaling of the fully coupled Terrestrial Systems Modeling Platform (TerrSysMP v1.0) in a massively parallel supercomputing environment – A case study on JUQUEEN (IBM Blue Gene/Q). *Geoscientific Model Development*, *7*(5), 2531–2543. https://doi.org/10.5194/gmd-7-2531-2014

Giorgi, F., Jones, C., & Asrar, G. R. (2009). Addressing climate information needs at the regional level: The CORDEX framework. *World Meteorological Organization (WMO) Bulletin*, *58*(3), 175.

Graf, A., Klosterhalfen, A., Arriga, N., Bernhofer, C., Bogena, H., Bornet, F., et al. (2020). Altered energy partitioning across terrestrial ecosystems in the European drought year 2018. *Philosophical Transactions of the Royal Society B: Biological Sciences*, *375*(1810), 20190524. https://doi.org/10.1098/rstb.2019.0524

Guimberteau, M., Zhu, D., Maignan, F., Huang, Y., Yue, C., Dantec-Nédélec, S., et al. (2018). ORCHIDEE-MICT (v8.4.1), a land surface model for the high latitudes: Model description and validation. *Geoscientific Model Development*, *11*(1), 121–163. https://doi.org/10.5194/gmd-11-121-2018

Han, X., Franssen, H.-J. H., Montzka, C., & Vereecken, H. (2014). Soil moisture and soil properties estimation in the Community Land Model with synthetic brightness temperature observations. *Water Resources Research*, *50*(7), 6081–6105. https://doi.org/10.1002/2013wr014586

Heiskanen, J., Brümmer, C., Buchmann, N., Calfapietra, C., Chen, H., Gielen, B., et al. (2022). The integrated carbon observation system in Europe. *Bulletin of the American Meteorological Society*, *103*(3), E855–E872. https://doi.org/10.1175/bams-d-19-0364.1

Hersbach, H., Bell, B., Berrisford, P., Hirahara, S., Horányi, A., Muñoz-Sabater, J., et al. (2020). The ERA5 global reanalysis. *Quarterly Journal of the Royal Meteorological Society*, *146*(730), 1999–2049. https://doi.org/10.1002/qj.3803

HPSCTerrSys. (2024a). HPSCTerrSys/eCLM: Fork of community land model v5.0 [Software]. Retrieved from https://github.com/HPSCTerrSys/eCLM

HPSCTerrSys. (2024b). HPSCTerrSys/TSMP2: CMake-based TerrSysMP [Software]. Retrieved from https://github.com/HPSCTerrSys/TSMP2

Hwang, T., Gholizadeh, H., Sims, D. A., Novick, K. A., Brzostek, E. R., Phillips, R. P., et al. (2017). Capturing species-level drought responses in a temperate deciduous forest using ratios of photochemical reflectance indices between sunlit and shaded canopies. *Remote Sensing of Environment*, *199*, 350–359. https://doi.org/10.1016/j.rse.2017.07.033

ICOS RI. (2022). Ecosystem final quality (L2) product in ETC-archive format - Release 2022-1 [Dataset]. https://doi.org/10.18160/PAD9-HQHU

Jasechko, S., Sharp, Z. D., Gibson, J. J., Birks, S. J., Yi, Y., & Fawcett, P. J. (2013). Terrestrial water fluxes dominated by transpiration. *Nature*, *496*(7445), 347–350. https://doi.org/10.1038/nature11983

Jefferson, J. L., Maxwell, R. M., & Constantine, P. G. (2017). Exploring the sensitivity of photosynthesis and stomatal resistance parameters in a land surface model. *Journal of Hydrometeorology*, *18*(3), 897–915. https://doi.org/10.1175/jhm-d-16-0053.1

Kaandorp, M. (2026a). eCLM release for "History Matching of Soil Moisture and Evapotranspiration over Europe using Iterative Ensemble Smoothers" [Software]. https://doi.org/10.5281/zenodo.19912983

Kaandorp, M. (2026b). Repository release for "History Matching of Soil Moisture and Evapotranspiration over Europe using Iterative Ensemble Smoothers" [Software]. https://doi.org/10.5281/zenodo.19912810

Köpke, C., Elsheikh, A. H., & Irving, J. (2019). Hydrogeophysical parameter estimation using iterative ensemble smoothing and approximate forward solvers. *Frontiers in Environmental Science*, *7*, 34. https://doi.org/10.3389/fenvs.2019.00034

Koster, R. D., Dirmeyer, P. A., Guo, Z., Bonan, G., Chan, E., Cox, P., et al. (2004). Regions of strong coupling between soil moisture and precipitation. *Science*, *305*(5687), 1138–1140. https://doi.org/10.1126/science.1100217

Koster, R. D., Reichle, R. H., Schubert, S. D., & Mahanama, S. P. (2019). Length scales of hydrological variability as inferred from SMAP soil moisture retrievals. *Journal of Hydrometeorology*, *20*(11), 2129–2146. https://doi.org/10.1175/jhm-d-19-0070.1

Lannoy, G. J. M. D., & Reichle, R. H. (2016). Global assimilation of multiangle and multipolarization SMOS brightness temperature observations into the GEOS-5 catchment land surface model for soil moisture estimation. *Journal of Hydrometeorology*, *17*(2), 669–691. https://doi.org/10.1175/jhm-d-15-0037.1

Largeron, C., Dumont, M., Morin, S., Boone, A., Lafaysse, M., Metref, S., et al. (2020). Toward snow cover estimation in mountainous areas using modern data assimilation methods: A review. *Frontiers in Earth Science*, *8*, 325. https://doi.org/10.3389/feart.2020.00325

Lavers, D. A., Simmons, A., Vamborg, F., & Rodwell, M. J. (2022). An evaluation of ERA5 precipitation for climate monitoring. *Quarterly Journal of the Royal Meteorological Society*, *148*(748), 3152–3165. https://doi.org/10.1002/qj.4351

Lawrence, D. M., Fisher, R. A., Koven, C. D., Oleson, K. W., Swenson, S. C., Bonan, G., et al. (2019). The community land model version 5: Description of new features, benchmarking, and impact of forcing uncertainty. *Journal of Advances in Modeling Earth Systems*, *11*(12), 4245–4287. https://doi.org/10.1029/2018ms001583

Lawrence, D. M., & Slater, A. G. (2008). Incorporating organic soil into a global climate model. *Climate Dynamics*, *30*(2), 145–160. https://doi.org/10.1007/s00382-007-0278-1

Letts, M. G., Roulet, N. T., Comer, N. T., Skarupa, M. R., & Verseghy, D. L. (2000). Parametrization of peatland hydraulic properties for the Canadian land surface scheme. *Atmosphere-Ocean*, *38*(1), 141–160. https://doi.org/10.1080/07055900.2000.9649643

Li, J., Duan, Q. Y., Gong, W., Ye, A., Dai, Y., Miao, C., et al. (2013). Assessing parameter importance of the Common Land Model based on qualitative and quantitative sensitivity analysis. *Hydrology and Earth System Sciences*, *17*(8), 3279–3293. https://doi.org/10.5194/hess-17-3279-2013

Li, M., Su, Y., Song, Q., Zhang, Y., Gao, H., Dong, J., & Shao, W. (2024). Identified temporal variation of soil hydraulic parameters under seasonal ecosystem change using the particle batch smoother. *Geoderma*, *442*, 116782. https://doi.org/10.1016/j.geoderma.2024.116782

Lievens, H., Tomer, S. K., Al Bitar, A., De Lannoy, G. J. M., Drusch, M., Dumedah, G., et al. (2015). SMOS soil moisture assimilation for improved hydrologic simulation in the Murray Darling Basin, Australia. *Remote Sensing of Environment*, *168*, 146–162. https://doi.org/10.1016/j.rse.2015.06.025

Loaiza Usuga, J. C., & Pauwels, V. R. N. (2008). Calibration and multiple data set-based validation of a land surface model in a mountainous Mediterranean study area. *Journal of Hydrology*, *356*(1), 223–233. https://doi.org/10.1016/j.jhydrol.2008.04.018

Malartic, Q., Farchi, A., & Bocquet, M. (2022). State, global and local parameter estimation using local ensemble Kalman filters: Applications to online machine learning of chaotic dynamics. *Quarterly Journal of the Royal Meteorological Society*, *148*(746), 2167–2193. https://doi.org/10.1002/qj.4297

Markonis, Y., Kumar, R., Hanel, M., Rakovec, O., Máca, P., & AghaKouchak, A. (2021). The rise of compound warm-season droughts in Europe. *Science Advances*, *7*(6), eabb9668. https://doi.org/10.1126/sciadv.abb9668

Medlyn, B. E., Duursma, R. A., Eamus, D., Ellsworth, D. S., Prentice, I. C., Barton, C. V. M., et al. (2011). Reconciling the optimal and empirical approaches to modelling stomatal conductance. *Global Change Biology*, *17*(6), 2134–2144. https://doi.org/10.1111/j.1365-2486.2010.02375.x

Montzka, C., Bogena, H. R., Zreda, M., Monerris, A., Morrison, R., Muddu, S., & Vereecken, H. (2017). Validation of spaceborne and modelled surface soil moisture products with Cosmic-Ray Neutron Probes. *Remote Sensing*, *9*(2), 103. https://doi.org/10.3390/rs9020103

Montzka, C., Moradkhani, H., Weihermüller, L., Franssen, H.-J. H., Canty, M., & Vereecken, H. (2011). Hydraulic parameter estimation by remotely-sensed top soil moisture observations with the particle filter. *Journal of Hydrology*, *399*(3), 410–421. https://doi.org/10.1016/j.jhydrol.2011.01.020

Moradkhani, H., Sorooshian, S., Gupta, H. V., & Houser, P. R. (2005). Dual state–parameter estimation of hydrological models using ensemble Kalman filter. *Advances in Water Resources*, *28*(2), 135–147. https://doi.org/10.1016/j.advwatres.2004.09.002

Muñoz-Sabater, J., Lawrence, H., Albergel, C., Rosnay, P., Isaksen, L., Mecklenburg, S., et al. (2019). Assimilation of SMOS brightness temperatures in the ECMWF Integrated Forecasting System. *Quarterly Journal of the Royal Meteorological Society*, *145*(723), 2524–2548. https://doi.org/10.1002/qj.3577

Naumann, G., Cammalleri, C., Mentaschi, L., & Feyen, L. (2021). Increased economic drought impacts in Europe with anthropogenic warming. *Nature Climate Change*, *11*(6), 485–491. https://doi.org/10.1038/s41558-021-01044-3

Naz, B. S., Sharples, W., Ma, Y., Goergen, K., & Kollet, S. (2023). Continental-scale evaluation of a fully distributed coupled land surface and groundwater model, ParFlow-CLM (v3.6.0), over Europe. *Geoscientific Model Development*, *16*(6), 1617–1639. https://doi.org/10.5194/gmd-16-1617-2023

Niu, G.-Y., Yang, Z.-L., Dickinson, R. E., & Gulden, L. E. (2005). A simple TOPMODEL-based runoff parameterization (SIMTOP) for use in global climate models. *Journal of Geophysical Research*, *110*(D21). https://doi.org/10.1029/2005jd006111

Nykanen, D. K., & Foufoula-Georgiou, E. (2001). Soil moisture variability and scale-dependency of nonlinear parameterizations in coupled land–atmosphere models. *Advances in Water Resources*, *24*(9), 1143–1157. https://doi.org/10.1016/s0309-1708(01)00046-x

O'Neill, P. E., Chan, S., Njoku, E., Jackson, T., Bindlish, R., & Chaubell, J. (2020). SMAP Enhanced L3 Radiometer Global Daily 9 km EASE-Grid Soil Moisture, version 4 [Dataset]. *Boulder, Colorado USA. NASA National Snow and Ice Data Center Distributed Active Archive Center*. Retrieved from https://nsidc.org/data/SPL3SMP_E/versions/4

Park, C.-H., Montzka, C., Jagdhuber, T., Jonard, F., De Lannoy, G., Hong, J., et al. (2019). A dielectric mixing model accounting for soil organic matter. *Vadose Zone Journal*, *18*(1), 190036. https://doi.org/10.2136/vzj2019.04.0036

Pastorello, G., Trotta, C., Canfora, E., Chu, H., Christianson, D., Cheah, Y.-W., et al. (2020). The FLUXNET2015 dataset and the ONEFlux processing pipeline for eddy covariance data. *Scientific Data*, *7*(1), 225. https://doi.org/10.1038/s41597-020-0534-3

Patil, A., Fersch, B., Hendricks Franssen, H.-J., & Kunstmann, H. (2021). Assimilation of cosmogenic neutron counts for improved soil moisture prediction in a distributed land surface model. *Frontiers in Water*, *3*, 729592. https://doi.org/10.3389/frwa.2021.729592

Peters-Lidard, C. D., Kumar, S. V., Mocko, D. M., & Tian, Y. (2011). Estimating evapotranspiration with land data assimilation systems. *Hydrological Processes*, *25*(26), 3979–3992. https://doi.org/10.1002/hyp.8387

Peylin, P., Bacour, C., MacBean, N., Leonard, S., Rayner, P., Kuppel, S., et al. (2016). A new stepwise carbon cycle data assimilation system using multiple data streams to constrain the simulated land surface carbon cycle. *Geoscientific Model Development*, *9*(9), 3321–3346. https://doi.org/10.5194/gmd-9-3321-2016

Pinnington, E., Amezcua, J., Cooper, E., Dadson, S., Ellis, R., Peng, J., et al. (2021). Improving soil moisture prediction of a high-resolution land surface model by parameterising pedotransfer functions through assimilation of SMAP satellite data. *Hydrology and Earth System Sciences*, *25*(3), 1617–1641. https://doi.org/10.5194/hess-25-1617-2021

Pinnington, E., Quaife, T., Lawless, A., Williams, K., Arkebauer, T., & Scoby, D. (2020). The land variational ensemble data assimilation framework: LAVENDAR v1.0.0. *Geoscientific Model Development*, *13*(1), 55–69. https://doi.org/10.5194/gmd-13-55-2020

Poll, S., Rigor, P., Brdar, S., Ho-Hagemann, H. T. M., Hartick, C., van Hulten, M., et al. (2025). The new TSMP2 coupled Earth system model. *EGUsphere*. [Preprint]. https://doi.org/10.5194/egusphere-2025-5468

Poppe Terán, C., Naz, B. S., Graf, A., Qu, Y., Hendricks Franssen, H.-J., Baatz, R., et al. (2023). Rising water-use efficiency in European grasslands is driven by increased primary production. *Communications Earth & Environment*, *4*(1), 95. https://doi.org/10.1038/s43247-023-00757-x

Poppe Terán, C., Naz, B. S., Vereecken, H., Baatz, R., Fisher, R. A., & Hendricks Franssen, H.-J. (2025). Systematic underestimation of type-specific ecosystem process variability in the Community Land Model v5 over Europe. *Geoscientific Model Development*, *18*(2), 287–317. https://doi.org/10.5194/gmd-18-287-2025

Rafiee, J., & Reynolds, A. C. (2017). Theoretical and efficient practical procedures for the generation of inflation factors for ES-MDA. *Inverse Problems*, *33*(11), 115003. https://doi.org/10.1088/1361-6420/aa8cb2

Rakovec, O., Samaniego, L., Hari, V., Markonis, Y., Moravec, V., Thober, S., et al. (2022). The 2018–2020 multi-year drought sets a new benchmark in Europe. *Earth's Future*, *10*(3), e2021EF002394. https://doi.org/10.1029/2021ef002394

Raoult, N. M., Jupp, T. E., Cox, P. M., & Luke, C. M. (2016). Land-surface parameter optimisation using data assimilation techniques: The adJULES system V1.0. *Geoscientific Model Development*, *9*(8), 2833–2852. https://doi.org/10.5194/gmd-9-2833-2016

Rezaei, E. E., Webber, H., Asseng, S., Boote, K., Durand, J. L., Ewert, F., et al. (2023). Climate change impacts on crop yields. *Nature Reviews Earth & Environment*, *4*(12), 831–846. https://doi.org/10.1038/s43017-023-00491-0

Rodríguez-Fernández, N., de Rosnay, P., Albergel, C., Richaume, P., Aires, F., Prigent, C., & Kerr, Y. (2019). SMOS neural network soil moisture data assimilation in a land surface model and atmospheric impact. *Remote Sensing*, *11*(11), 1334. https://doi.org/10.3390/rs11111334

Rothfuss, Y., Quade, M., Brüggemann, N., Graf, A., Vereecken, H., & Dubbert, M. (2021). Reviews and syntheses: Gaining insights into evapotranspiration partitioning with novel isotopic monitoring methods. *Biogeosciences*, *18*(12), 3701–3732. https://doi.org/10.5194/bg-18-3701-2021

Rousi, E., Kornhuber, K., Beobide-Arsuaga, G., Luo, F., & Coumou, D. (2022). Accelerated western European heatwave trends linked to more-persistent double jets over Eurasia. *Nature Communications*, *13*(1), 3851. https://doi.org/10.1038/s41467-022-31432-y

Samaniego, L., Kumar, R., & Zink, M. (2013). Implications of parameter uncertainty on soil moisture drought analysis in Germany. *Journal of Hydrometeorology*, *14*(1), 47–68. https://doi.org/10.1175/jhm-d-12-075.1

Seneviratne, S. I., Corti, T., Davin, E. L., Hirschi, M., Jaeger, E. B., Lehner, I., et al. (2010). Investigating soil moisture–climate interactions in a changing climate: A review. *Earth-Science Reviews*, *99*(3), 125–161. https://doi.org/10.1016/j.earscirev.2010.02.004

Seo, E., Lee, M.-I., & Reichle, R. H. (2021). Assimilation of SMAP and ASCAT soil moisture retrievals into the JULES land surface model using the Local Ensemble Transform Kalman Filter. *Remote Sensing of Environment*, *253*, 112222. https://doi.org/10.1016/j.rse.2020.112222

Sepulchre, P., Caubel, A., Ladant, J.-B., Bopp, L., Boucher, O., Braconnot, P., et al. (2020). IPSL-CM5A2 – An Earth system model designed for multi-millennial climate simulations. *Geoscientific Model Development*, *13*(7), 3011–3053. https://doi.org/10.5194/gmd-13-3011-2020

Shangguan, W., Hengl, T., Mendes de Jesus, J., Yuan, H., & Dai, Y. (2017). Mapping the global depth to bedrock for land surface modeling. *Journal of Advances in Modeling Earth Systems*, *9*(1), 65–68. https://doi.org/10.1002/2016ms000686

Shrestha, P., Sulis, M., Masbou, M., Kollet, S., & Simmer, C. (2014). A scale-consistent terrestrial systems modeling platform based on COSMO, CLM, and ParFlow. *Monthly Weather Review*, *142*(9), 3466–3483. https://doi.org/10.1175/mwr-d-14-00029.1

Silva, T. M. D., Pesco, S., & Barreto, A. (2021). Influences of the inflation factors generation in the main parameters of the ensemble smoother with multiple data assimilation. *Journal of Petroleum Science and Engineering*, *203*, 108648. https://doi.org/10.1016/j.petrol.2021.108648

Sitch, S., Friedlingstein, P., Gruber, N., Jones, S. D., Murray-Tortarolo, G., Ahlström, A., et al. (2015). Recent trends and drivers of regional sources and sinks of carbon dioxide. *Biogeosciences*, *12*(3), 653–679. https://doi.org/10.5194/bg-12-653-2015

Song, J., Miller, G. R., Cahill, A. T., Aparecido, L. M. T., & Moore, G. W. (2020). Modeling land surface processes over a mountainous rainforest in Costa Rica using CLM4.5 and CLM5. *Geoscientific Model Development*, *13*(11), 5147–5173. https://doi.org/10.5194/gmd-13-5147-2020

Stoorvogel, J. J., & Mulder, V. L. (2021). A comparison, validation, and evaluation of the S-world global soil property database. *Land*, *10*(5), 544. https://doi.org/10.3390/land10050544

Strebel, L., Bogena, H., Vereecken, H., Andreasen, M., Aranda-Barranco, S., & Hendricks Franssen, H.-J. (2024). Evapotranspiration prediction for European forest sites does not improve with assimilation of in situ soil water content data. *Hydrology and Earth System Sciences*, *28*(4), 1001–1026. https://doi.org/10.5194/hess-28-1001-2024

Tyree, M. T., & Sperry, J. S. (1989). Vulnerability of Xylem to cavitation and embolism. *Annual Review of Plant Physiology and Plant Molecular Biology*, *40*(1), 19–36. https://doi.org/10.1146/annurev.pp.40.060189.000315

Umair, M., Kim, D., & Choi, M. (2020). Impact of climate, rising atmospheric carbon dioxide, and other environmental factors on water-use efficiency at multiple land cover types. *Scientific Reports*, *10*(1), 11644. https://doi.org/10.1038/s41598-020-68472-7

van der Velde, R., Colliander, A., Pezij, M., Benninga, H.-J. F., Bindlish, R., Chan, S. K., et al. (2021). Validation of SMAP L2 passive-only soil moisture products using upscaled in situ measurements collected in Twente, the Netherlands. *Hydrology and Earth System Sciences*, *25*(1), 473–495. https://doi.org/10.5194/hess-25-473-2021

Vogel, M. M., Zscheischler, J., Wartenburger, R., Dee, D., & Seneviratne, S. I. (2019). Concurrent 2018 hot extremes across Northern Hemisphere due to human-induced climate change. *Earth's Future*, *7*(7), 692–703. https://doi.org/10.1029/2019ef001189

Warm Winter 2020 Team and ICOS Ecosystem Thematic Centre. (2022). Warm Winter 2020 ecosystem eddy covariance flux product for 73 stations in FLUXNET-Archive format—Release 2022-1 [Dataset]. Medium: Collection of FLUXNET product ZIP archives Publisher: ICOS Carbon Portal Version Number: 1.0.

Wozniak, M. C., Bonan, G. B., Keppel-Aleks, G., & Steiner, A. L. (2020). Influence of vertical heterogeneities in the canopy microenvironment on interannual variability of carbon uptake in temperate deciduous forests. *Journal of Geophysical Research: Biogeosciences*, *125*(8), e2020JG005658. https://doi.org/10.1029/2020jg005658

Wu, G., Guan, K., Li, Y., Novick, K. A., Feng, X., McDowell, N. G., et al. (2021). Interannual variability of ecosystem iso/anisohydry is regulated by environmental dryness. *New Phytologist*, *229*(5), 2562–2575. https://doi.org/10.1111/nph.17040

Xie, X., Li, A., Tan, J., Lei, G., Jin, H., & Zhang, Z. (2020). Uncertainty analysis of multiple global GPP datasets in characterizing the lagged effect of drought on photosynthesis. *Ecological Indicators*, *113*, 106224. https://doi.org/10.1016/j.ecolind.2020.106224

Yan, H., Sun, N., Eldardiry, H., Thurber, T. B., Reed, P. M., Malek, K., et al. (2023a). Large ensemble diagnostic evaluation of hydrologic parameter uncertainty in the community land model version 5 (CLM5). *Journal of Advances in Modeling Earth Systems*, *15*(5), e2022MS003312. https://doi.org/10.1029/2022MS003312

Yan, H., Sun, N., Eldardiry, H., Thurber, T. B., Reed, P. M., Malek, K., et al. (2023b). Characterizing uncertainty in Community Land Model version 5 hydrological applications in the United States. *Scientific Data*, *10*(1), 187. https://doi.org/10.1038/s41597-023-02049-7

Yi, Y., Chen, R. H., Kimball, J. S., Moghaddam, M., Xu, X., Euskirchen, E. S., et al. (2022). Potential satellite monitoring of surface organic soil properties in Arctic Tundra from SMAP. *Water Resources Research*, *58*(4), e2021WR030957. https://doi.org/10.1029/2021WR030957

Zängl, G., Reinert, D., Rípodas, P., & Baldauf, M. (2015). The ICON (ICOsahedral Non-hydrostatic) modelling framework of DWD and MPI-M: Description of the non-hydrostatic dynamical core. *Quarterly Journal of the Royal Meteorological Society*, *141*(687), 563–579. https://doi.org/10.1002/qj.2378

Zhang, W., Koch, J., Wei, F., Zeng, Z., Fang, Z., & Fensholt, R. (2023). Soil moisture and atmospheric aridity impact spatio-temporal changes in evapotranspiration at a global scale. *Journal of Geophysical Research: Atmospheres*, *128*(8), e2022JD038046. https://doi.org/10.1029/2022jd038046

Zhang, W., Nelson, J. A., Miralles, D. G., Mauder, M., Migliavacca, M., Poyatos, R., et al. (2024). A new post-hoc method to reduce the energy imbalance in eddy covariance measurements. *Geophysical Research Letters*, *51*(2), e2023GL107084. https://doi.org/10.1029/2023gl107084

Zhang, Z., Guan, H., Veneklaas, E., Singha, K., & Batelaan, O. (2025). Revealing seasonal plasticity of whole-plant hydraulic properties using sap-flow and stem water-potential monitoring. *Hydrology and Earth System Sciences*, *29*(16), 3975–3992. https://doi.org/10.5194/hess-29-3975-2025

Zhao, H., Zeng, Y., Han, X., & Su, Z. (2023). Retrieving soil physical properties by assimilating SMAP brightness temperature observations into the community land model. *Sensors*, *23*(5), 2620. https://doi.org/10.3390/s23052620

Zomer, R. J., Xu, J., & Trabucco, A. (2022). Version 3 of the global aridity index and potential evapotranspiration database. *Scientific Data*, *9*(1), 409. https://doi.org/10.1038/s41597-022-01493-1